

## CHAPTER III

### CALCULATION DETAILS



In this chapter, the thesis work is revealed thoroughly the theoretical calculation approach of QD structure via **Matlab® programming language**. This structure is modeled by using the mathematics concepts related to quantum mechanics theorem. In addition, numerical method is introduced to simplify the computation with more accuracy. The calculation procedures are separated in two main parts. The first part is described about the investigation of self-assembled aligned QD structure by focusing on interdot coupling effects and correlation behind them. The second part represents an electric field on two-dimensional system taking into account to apply with the QD. Both parts are verified the results by utilizing another program, namely, **COMSOL Multiphysics**, to obtain the more precise results. Then, combines all of these parts for simulation the electric field effect on the optical polarization of self-assembled InAs aligned QDs. The calculation results will be shown and discussed in chapter 4.

### 3.1 SIMULATION OF THE SELF-ASSEMBLED ALIGNED QUANTUM DOTS

#### 3.1.1 Mathematical Model

In the structural characterization, the QDs model is developed base on the binary rectangular QDs reported in [207], then expansion to aligned QDs. The AFM images of this structure were used as a reference structure for building the aligned QD system as shown in **Figure 3.1 (a)**. According to the top view of AFM image, The aligned InAs QDs with circular shape were embedded in the GaAs surrounding matrix (GaAs capping layer). In the calculation, rectangular QD was used corresponding to the reasons mentioned in chapter 2.

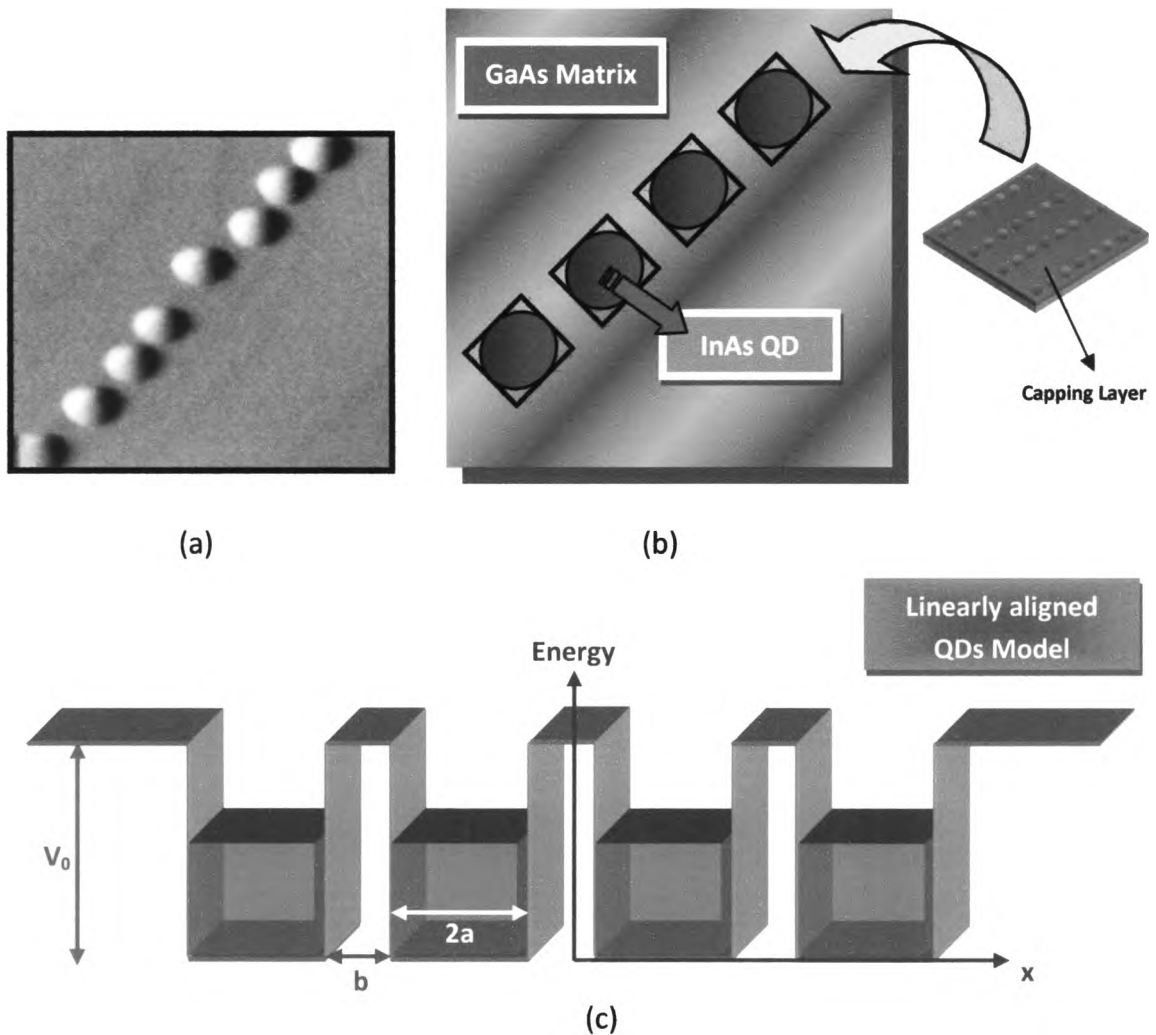


**Figure 3.1** Schematic diagram of InAs/GaAs linearly aligned quantum dots shown by AFM image (top view) [208]. (b) The mathematical model corresponding to AFM image and (c) band diagram related with.

It was assumed for simplicity that all the QDs had the same size with the same spacing between them, and confined in the periodic multiple quantum wells. **Figure 3.1 (b)** depicts the mathematical QDs model consists of InAs QDs and the potential barriers is the GaAs capping-layer material. Generally, the PL luminescence mostly emits from the recombination between electrons and heavy holes in the ground state, so only the ground-state eigen-energy levels will be focus for simplicity in calculation.

### 3.1.2 Theory

The calculations were performed using a band diagram in **Figure 3.1 (c)**. Each rectangular QD was embedded in the rectangular well width of size  $2a$ , the barrier width  $b$ , and the barrier height  $V_0$  (potential) in Cartesian coordinate system. Since recombination of carriers is assumed to be occurred in the ground state, the calculation was focused only on the ground-state eigen-energies ( $E_0$ ). To investigate the carriers distribution, the eigen-energy (eigenvalue) and the eigen-function (wavefunction) of a single carrier in semiconductor linearly aligned QDs must be achieved by the time-independent Schrödinger equation:

$$H\psi(x) = \left[ -\frac{\hbar^2}{2m^*} \frac{\partial^2}{\partial x^2} + V(x) \right] \psi(x) = E\psi(x) \quad (3.1)$$

where  $\psi(x)$  is the wavefunction distribution of carrier.  $m^*$  is the effective mass of the considered particles (electron or hole, depended on the band structure) and  $\hbar$  is the Planck's constant.  $V(x)$  is the difference between the bandgap energy between InAs quantum dots and the GaAs surrounding matrix. The corresponding values are 1.12 eV and 1.43 eV, respectively at room temperature [209-210] with the condition:

$$V(x) = \begin{cases} 0 & \left\{ \begin{array}{l} x \in QDs \\ x \notin QDs \end{array} \right. \\ V_0 & \end{cases} \quad (3.2)$$

$E$  is the eigen-energy of the system. Because the recombination of carriers occurs in the **bound states**, only the case for consideration is  $E < V_0$ .





### 3.1.3 Numerical Calculation in Two-Dimensional Rectangular Aligned QDs

This thesis work presents the model of rectangular aligned QDs in two-dimensional case. There are many reasons why the structure mention above is introduced as follows:

- In real QD structure, the complexity of calculation is described by the parameters, such as shape (many shape are designed) [70, 211], composition of substances [212, 213], and strain distribution [60, 162] which remain not clear in some information for deeply examination. This investigation allows for the research which highlight to the high accuracy in overall details as possible. On the other hand, it is not appropriate in the calculation which focuses only on the tendency of changing in some parameters roughly.

- In the case of calculation, because the precise results are required, the QD should be modeled in form of three-dimensional shape. Though this model can reach the real structure, it is essential to take a long time for calculation (i.e., five times or more compared with the lower dimensional structure). Furthermore, high performance of computer is required for increasing a calculation's efficiency.

**Table 3.1:** Comparison of the modeling of QD structure for three different dimensions.

Dimension	Shape Modeling	Data Details	Calculating Time	Computation Performance
1D	simple	Not many	Fast	Low
2D				
3D	Realistic	Many	Slow	High

For the limitations described above, the two-dimensional model is the best choice to compensate between one-dimensional (short time calculation, but low accuracy) and three-dimensional model (high accuracy, but long time calculation).

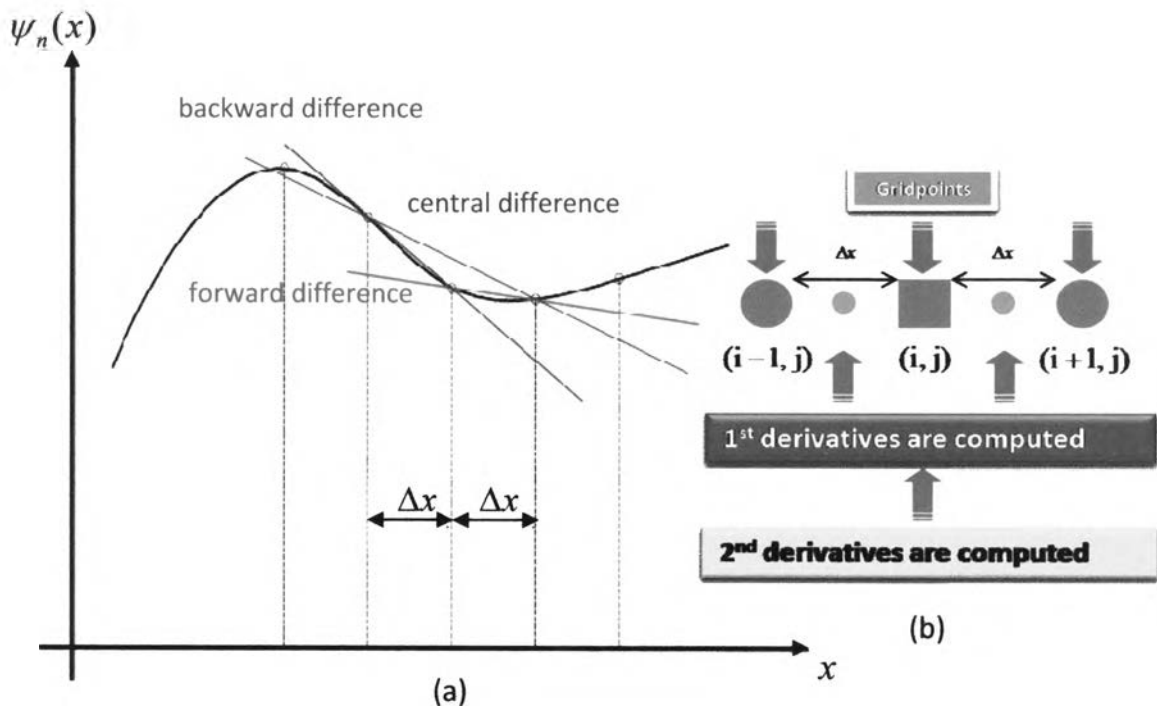


**Figure 3.2** Illustration of (a) finite-difference approximation by different geometric interpretations of the first-order finite difference approximation related to forward, backward, and central difference approximation. (b) Simple diagram of reduction from high order derivatives to lower order derivatives.

In many quantum mechanics problem, the numerical methods were introduced for solving the solution which can't be evaluated by analytical methods. Here, one of the numerical technique used in thesis work is the **finite difference method (FDM)** [214-215] written in the Matlab® programming language. Because the time-independent Schrödinger equation is a second-order differential equation that satisfies the appropriate boundary conditions, the FDM method is proper to approximate the solutions of differential equations by replacing derivative expressions with approximately equivalent difference quotients. FDM schemes for

high order derivatives can be obtained from the formulas for lower order derivatives. Then, solving the problem with boundary condition to give information of carrier distribution. Moreover, the considered structure is two-dimensional, so the FDM method is more directly related than the finite-element method which is generally used in three-dimensional problem.

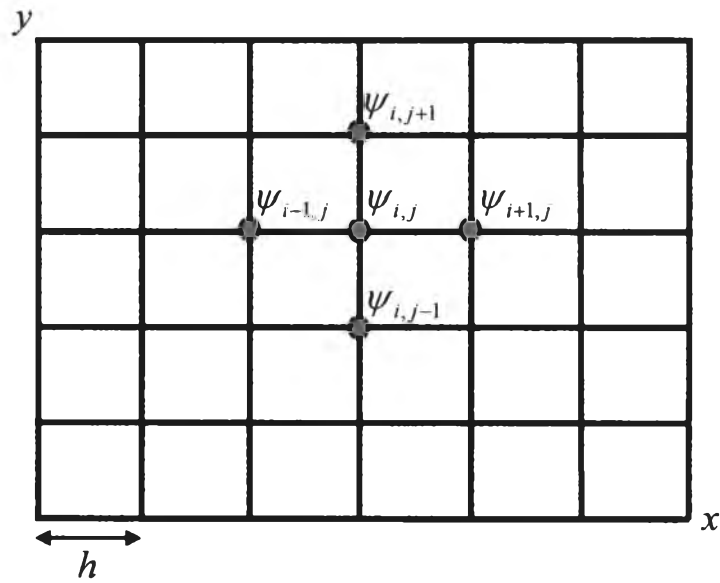


**Figure 3.3** The discretized mesh points for the two-dimensional Schrödinger equation.

By using FDM method as reported in [207], The wavefunction and the potential were discretized into many small grid points such that the  $x$  coordinates becomes  $x_i = ih_0$ , index  $i = 0, 1, 2, 3, 4, \dots$ ,  $h_0$  is the distance between the adjacent grid points as shown in **Figure 3.3**. Thus, the two-dimensional Schrödinger equation was changed into the two-dimensional finite-difference form:

$$-\frac{\hbar^2}{2m^*h_0^2} \left[ \{\psi_{i-1,j} - 2\psi_{i,j} + \psi_{i+1,j}\} - 2\psi_{i,j} + \{\psi_{i,j-1} - 2\psi_{i,j} + \psi_{i,j+1}\} \right] + V_j \psi_{i,j} = E \psi_{i,j} \quad (3.3)$$



### 3.1.4 Results and Discussion

#### 3.1.4.1 Comparison and verification the results calculated between two programs

Calculations were performed using Matlab® programming language to numerically solve the two-dimensional Schrödinger equation by FDM method with appropriate boundary conditions, results in wavefunction (eigen-functions) and corresponding eigen-energy value of the system. Because a band structure in the system composes of conduction band valence band, different effective mass values (electron and hole) were used to give both electron and hole wavefunctions for calculating the optical intensity of carrier recombination. This will be applied to estimate a polarization degree, which was demonstrated on next section. The effective mass values were shown in **Table 3.2**. To get close a real band structure, we used the ratio between conduction band ( $\Delta E_c$ ) and valence band ( $\Delta E_v$ ) offset (height of total potential difference) is proportional 70% to  $\Delta E_c$  and 30% to  $\Delta E_v$ , as shown in **Figure 3.4** [217].

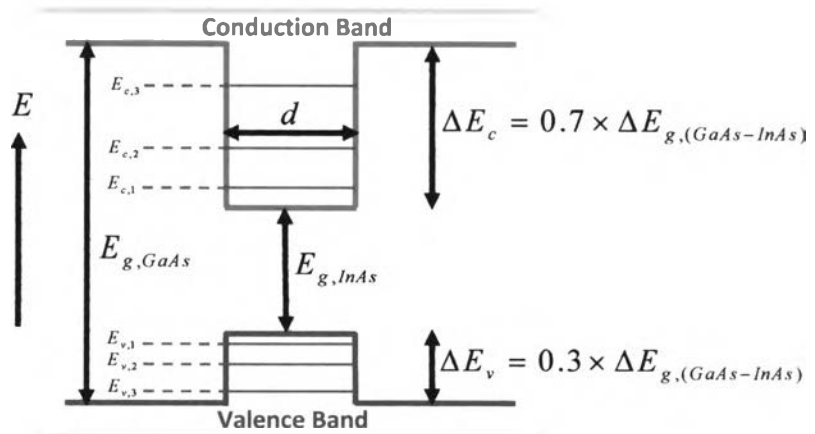


**Figure 3.4** Illustration of the band gaps in the QD material InAs and the embedding material GaAs with ratio between  $\Delta E_c$  and  $\Delta E_v$  is 0.7 : 0.3.



**Table 3.2:** The effective electron and heavy hole mass parameters ( $m_e$  is electron mass) [218-219].

Region	$m_e^*$	$m_h^*$
GaAs	0.0667 $m_e$	0.34 $m_e$
InAs	0.0234 $m_e$	0.33 $m_e$

This computer program is quite flexible because it allows to make fine adjustment of some considerable parameters, such as size of QDs (horizontal and vertical), distance between adjacent QDs, number of QDs, particularly the number of mesh points in the system. Checking an accuracy of numerical method, we found that the maximum number of available mesh points before program displays a “out of memory” message [220] when calculating the Schrödinger equation was the square matrix with dimension of 3481x3481. Since the values of matrix elements in wavefunction solved from Schrödinger equation are great number of zero values, so it is called “sparse matrix”. Fortunately, Matlab® programming language has a “sparse matrix algorithm” [221] which aims to reduce a memory usage from the operating system when it is calculating. Applying the sparse function to each submatrix of Eq. (3.5), then combine these matrixes again and solve the equation in order to obtain wavefunction and corresponding eigen-energy value of the system. This technique can extend the number of mesh points reaching to 9801x9801 square matrix due to the limitation of optimization in Matlab® programming resource. Therefore, the maximum number of available QDs which can be calculated are 12 QDs. For simplicity in calculation, only even number of QDs was computed which is so accurately that can estimate the tendency of calculation results.

**Figure 3.5** manifest the shape of the wavefunctions resulting from the solution in Eq. (3.5) of four coupled QDs with three difference dot separation values. The size of each QD is 12x12 nm<sup>2</sup> (square-shaped QDs). The uniform mesh was used in the x and y directions and 2 nm was equivalent to 1 mesh ( $h$  value in **Figure 3.3**).

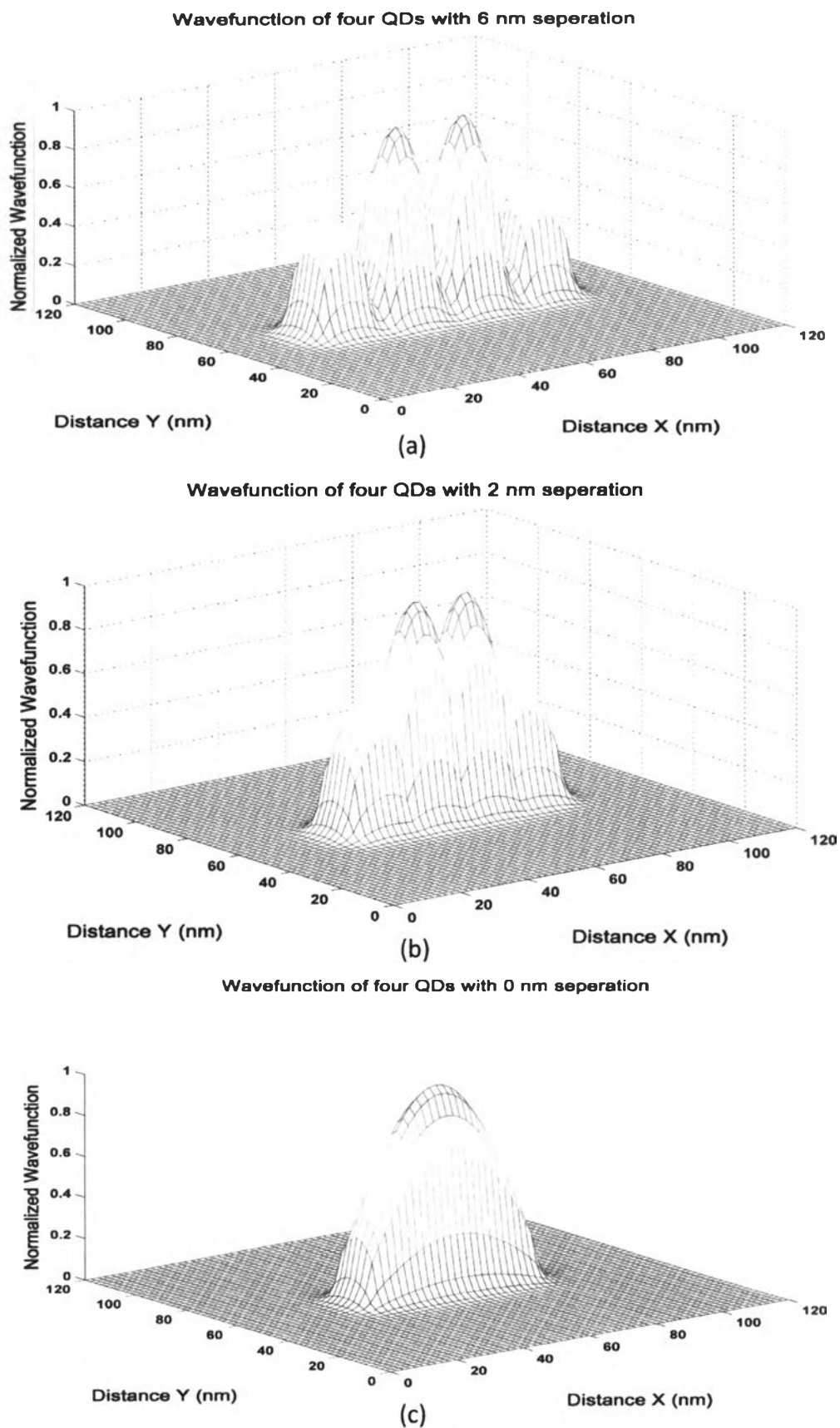


**Figure 3.5** Schematic diagram of coupling behavior of four coupled QDs with dot separation (a) 6 nm, (b) 2 nm, and (c) 0 nm (calculated by Matlab®).

We used “eigen-function” [222] in Matlab® command with the FDM method to solve the Schrödinger equation. As a result, we got the eigen-energy value and the corresponding eigen-functions. Note that this eigen-energy value is the ground-state eigen-energies as mentioned previously. In these cases, the coupling behavior of QDs can be clearly seen from the shape of the wavefunctions. When the dot separation is 6 nm, QDs are close enough to each other so that coupling between them already seen, as in the **Figure 3.5 (a)**. When the dot separation becomes smaller (2 nm, as shown in **Figure 3.5 (b)**), coupling between the dots becomes more pronounced. In case distance between QDs is 0 nm or the barrier width of each QD is zero (no barrier), all the quantum wells coalesce and become a single long potential well, and QD system looks like a quantum wire. In other words, the wavefunction of each QD completely fuses together and becomes a one larger Gaussian distribution curve, as depicted in **Figure 3.5 (c)**.

### **Comparison with COMSOL results**

As we introduce briefly at the beginning part of this chapter, **COMSOL Multiphysics** was introduced to make an expression, which can be compared with some numerically calculated results from Matlab® programming language. COMSOL Multiphysics is an excellent software for the solution of many types of partial differential equations (PDEs), both stationary and time-dependent, by numerical techniques based on the finite element method for the spatial discretization. It facilitates all steps in the modeling process - defining a geometry, meshing, specifying physics, solving, and visualizing the results. Furthermore, its versatility, flexibility and usability can easily be extended with its add-on modules.

COMSOL Multiphysics was applied to compare and test how precise about wave functions generated in Matlab® programming mentioned above. We used PDE (Partial Differential Equation), coefficient form model in PDE module to investigate the wave functions of four QDs. This was done by first drawing the four rectangular InAs QDs ( $12 \times 12 \text{ nm}^2$ ) with distance between them are 0, 2, and 6 nm (same as the

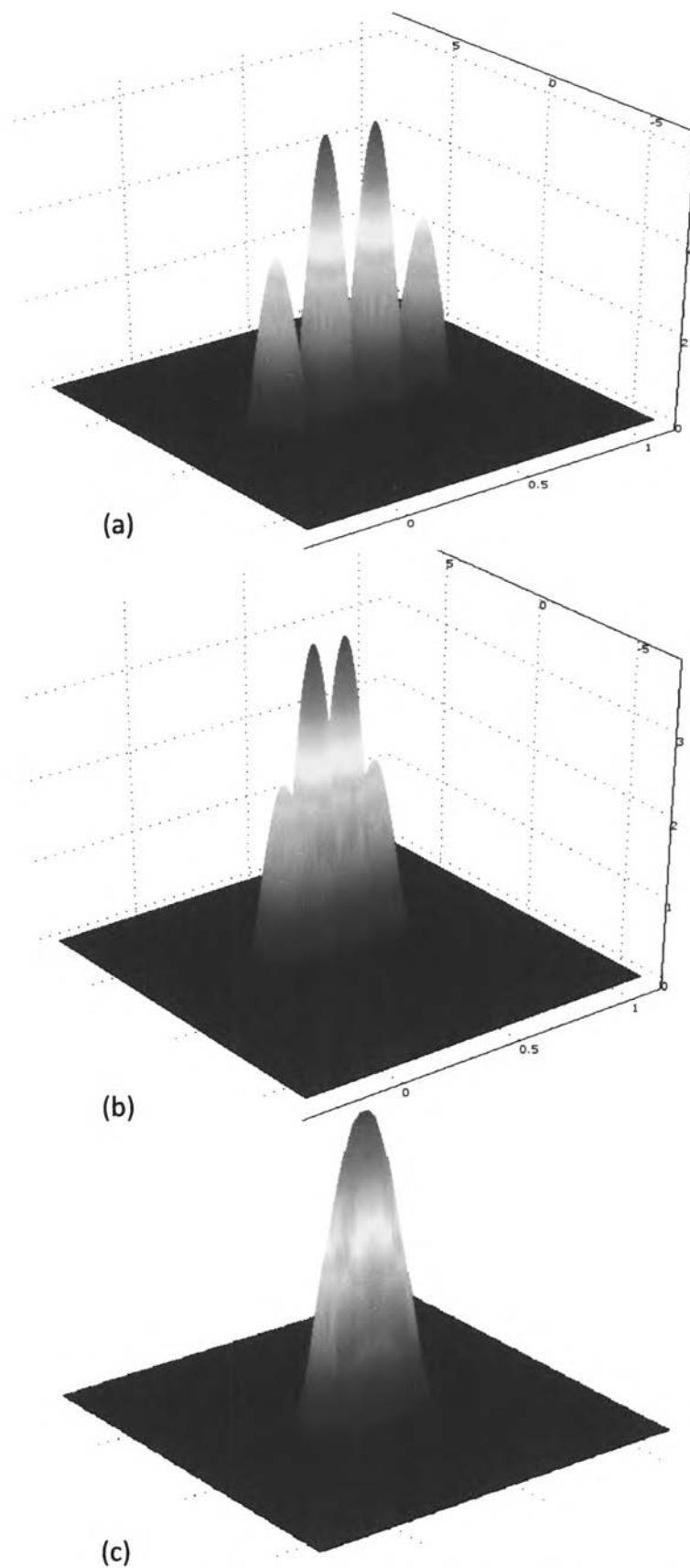


**Figure 3.6** Schematic diagram of coupling behavior of four coupled QDs with dot separation (a) 6 nm, (b) 2 nm, and (c) 0 nm (calculated by COMSOL).

**Table 3.3:** Comparison of ground-state eigen energy of four coupled QDs calculated by Matlab® programming and COMSOL Multiphysics.

Programming	Ground-state eigen-energy ( $E_0$ ) of four QDs with separation of		
	0 nm (eV)	2 nm (eV)	6 nm (eV)
Matlab®	0.0288	0.0742	0.0838
COMSOL	0.028776	0.073919	0.08378

previous cases calculated by Matlab® programming) surrounded by a larger two-dimensional square (GaAs region). The next step is to make a function by modifying some parameters of PDE, coefficient form changed to Eq. (3.1). The PDE, coefficient form can be written as:

$$\nabla \cdot (-c \nabla u - au + y) + au + b \cdot \nabla u = d_a \lambda u - e_a \lambda^2 u \quad (3.6)$$

Comparing with Eq. (3.5), we see that  $u = H$ ,  $\lambda = \psi$ ,  $d_a = 1$ ,  $c = \hbar^2 / (2m^*)$  ( $m^*$  values are difference for InAs QDs and GaAs region, see Table 3.3),  $a = 0$  (InAs QDs region) and 0.31 (GaAs region), and other parameters are set to zero value. Then inserting these into subdomains settings. With an appropriate boundary conditions, solving the problem by numerical calculation to obtain wavefunction and the corresponding eigen-energies. The results were shown in Figure 3.6. It was observed that the wavefunction distribution in each case of Figure 3.6 was similar to the results calculated in Figure 3.5. This was confirmed by comparison of ground-state eigen-energies calculated by two programs (see Table 3.3), which were slightly different (approximately < 0.002 %) indicating the exactitude of program computed by Matlab® programming language.

Some interesting aspect about the calculations and the results obtained above is the coupling effects which depend on separation between quantum dots. Especially the case of dot separation is zero (maximum coupling) the structure manifest a single long potential well implying that the increment of transition

probability of carriers in some certain direction. This is interesting for the polarization properties related to the energy splitting and coupling among aligned quantum dots which is delicately concentrated on next section.

### 3.1.4.2 Coupling effect on the linear optical polarization property

As mentioned previously in Chapter 2, polarization studies are a useful tool in giving some important information about the optical behavior of charge carriers in the QDs. A thorough understanding of this mechanism that can be used especially for measuring the direction of the intensity profile of emitted light. Thus, polarization plays an important role revealing an interesting optical property that require in many photonic devices. Polarization may be determined via optical intensity, which is directly related to transition probability of recombination phenomenon of carrier dynamics in emission process. For two-dimensional system, the optical intensity due to carrier transitions of the system may be found from the expression [223]:

$$I_{(\theta)}^{\nu} \propto \int \psi_i(x, y) r_{\theta} \psi_f(x, y) dx dy \quad (3.7)$$

where  $r$  stands for the coordinate of the optical transition,  $\theta$  stands for either the  $x$  or the  $y$  direction of polarization of light (considered in Cartesian coordinate system),  $\psi_i$  is the ground-state electron wavefunction (initially, electron carriers were excited by external photons, absorb them, and change state to conduction band momentarily), and  $\psi_f$  is the ground-state hole wavefunction (occurring from their electron pairs). By using the above equation, the degree of optical polarization anisotropy, or the “polarization degree” (PD) for two-dimensional systems may be determined as:

$$PD = \left| \frac{I_x - I_y}{I_x + I_y} \right| \quad (3.8)$$

where  $I_x$  and  $I_y$  are the emission optical intensity in  $x$  and  $y$  direction, respectively. Note that we concentrate on the case of linear polarization of two-dimensional system. To demonstrate and analyze the results, single QDs case will be described first, then extend to aligned QDs case, and finally give an overall conclusion.

#### 3.1.4.2.1 Single quantum dots

##### Increase of polarization degree with elongated QD

First of all, the ground-state wavefunctions of electron ( $\psi_i$ ) and hole ( $\psi_f$ ) were calculated by solving Schrödinger equation with the same method described in previous section. After that, using relation in (3.7) to find  $I_x$ ,  $I_y$  and taking them to Eq. (3.8) that yields the polarization degree of two-dimensional system. We considered a polarization degree of single isotropic shape QD ( $12 \times 12 \text{ nm}^2$ ) compared with elongated QD by size in the  $y$  direction was fixed to 12 nm and that in the  $x$  direction varied from 24 nm to 144 nm were investigated. The calculated electron wavefunction for isotropic QD and elongated QDs are shown in Figure 3.7. The results show that when the QD size is isotropic (dimension in the  $x$  and  $y$  directions are the same), the transition probability of both directions are the same. This result in producing an identity of polarization in all directions, that is, degree of polarization is zero. When the QD size is elongated in the  $x$  direction, now the transition probability in the  $x$  and the  $y$  direction are not the same. This allows carriers to moving mostly in the  $x$  direction causes to increasing  $I_x$  more than  $I_y$ . Thus, elongated QDs exhibit a certain degree of linear polarization ( $PD \neq 0$ ). Moreover, the larger size of elongated QD in the certain direction, the higher polarization degree gives.

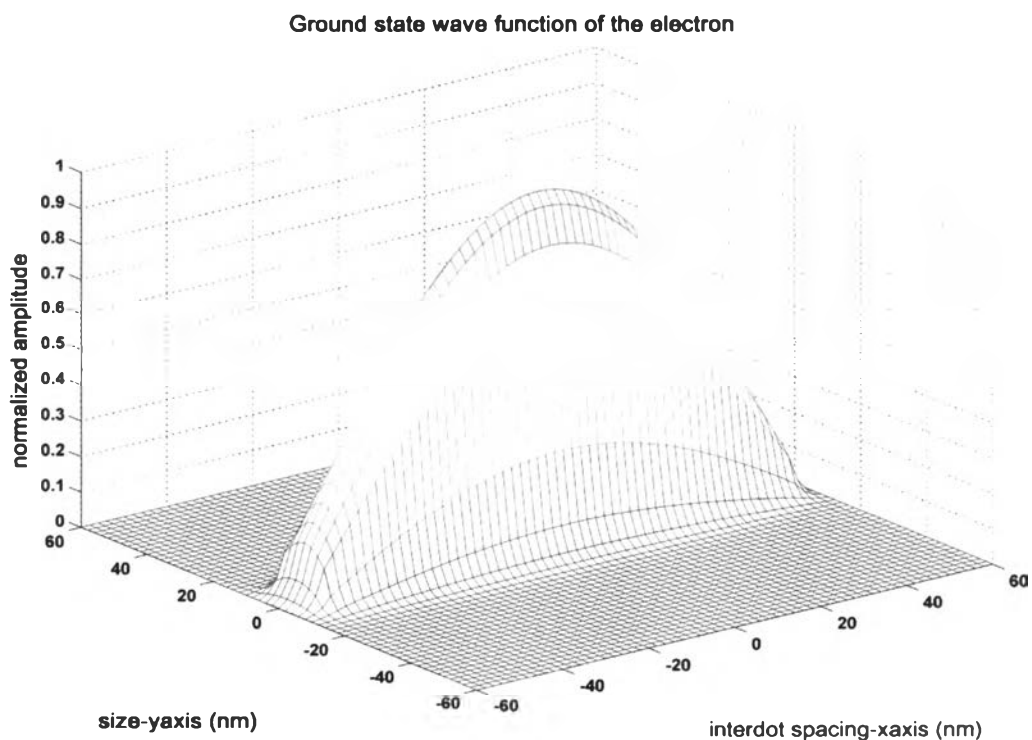
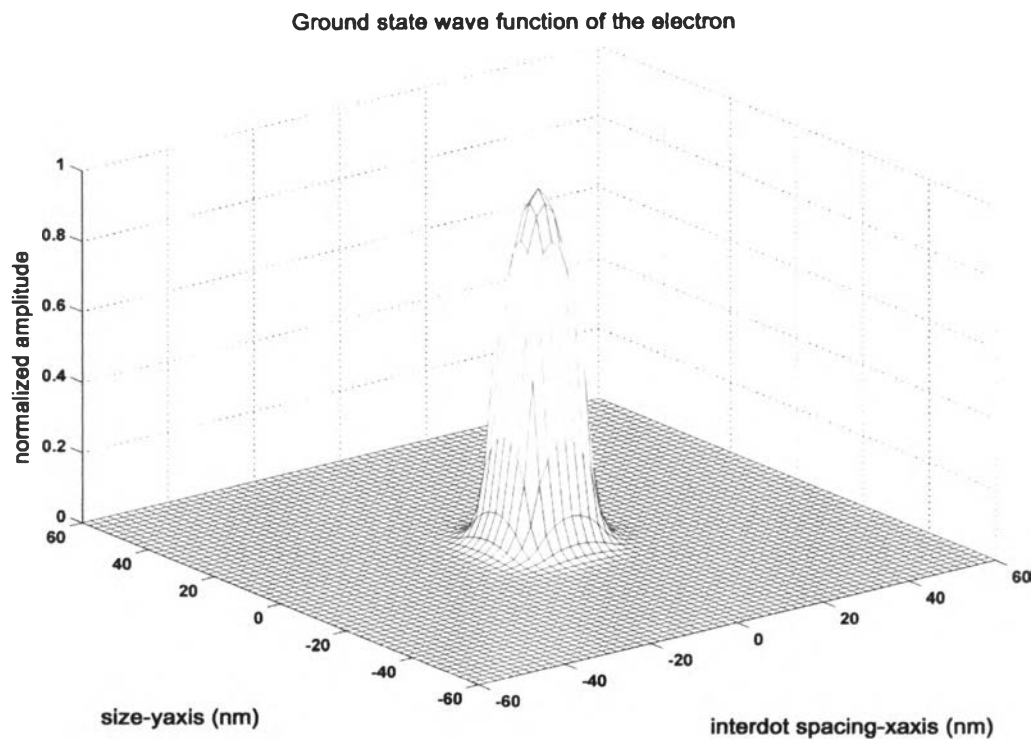


**Figure 3.7** The ground-state electron wavefunction of (a) isotropic single QD whose size is  $12 \times 12 \text{ nm}^2$  and (b) elongated QD (in x direction) with size of  $12 \times 108 \text{ nm}^2$ .



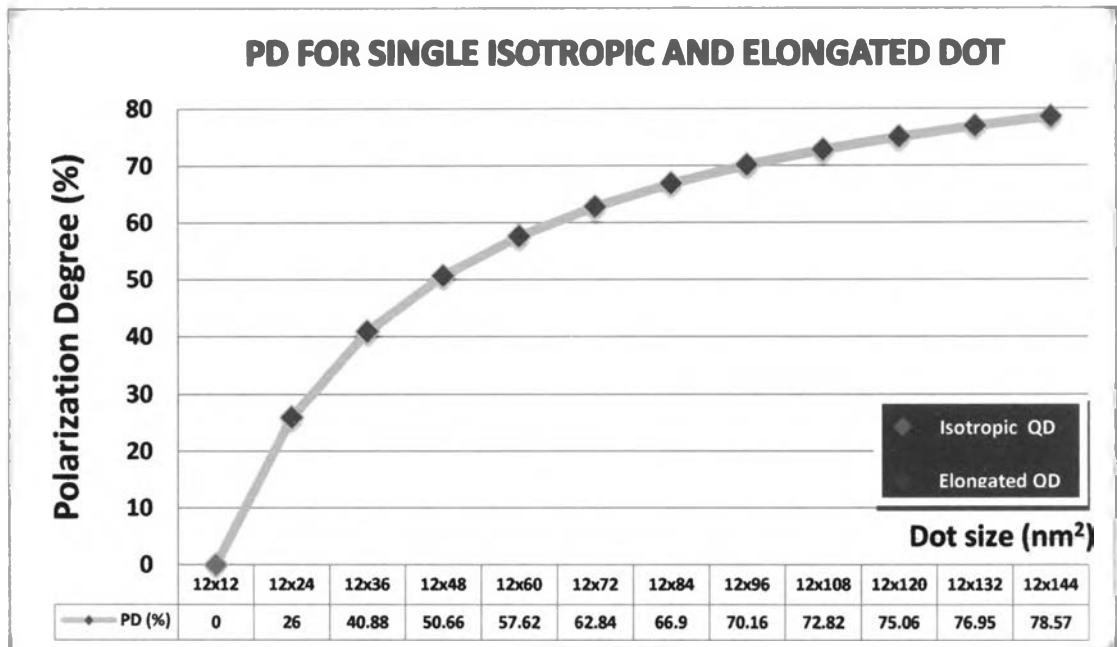


**Figure 3.8** The polarization degree of single QD whose size in the x direction was elongated from 12 to 144 nm while that in the y direction was maintained at 12 nm.

#### Comparison of aspect ratio on QD size with polarization degree

Next, the elongated QDs were considered with different sizes but the same aspect ratio. The amount of aspect ratio equal to 2, 3, 4, and 5 were calculated for analysis of polarization degree, as shown in **Figure 3.9**. For aspect ratio =2, as the size of QDs increase (both x and y direction), the PD also increase. In addition, degree of polarization goes up rapidly at the beginning until it slowly increases when the QD size is much larger than the primitive size. These were attributed to enlargement of wavefunction in both directions that enhances more and more transition probability in the x direction, and also enhances an optical intensity, result in PD increment. However, if the QD size is large enough at the one size, transition probability in the y direction begins dominant that will decelerate the increasing PD until its value saturates at the end. The results of other aspect ratios give a similar trend, as well.

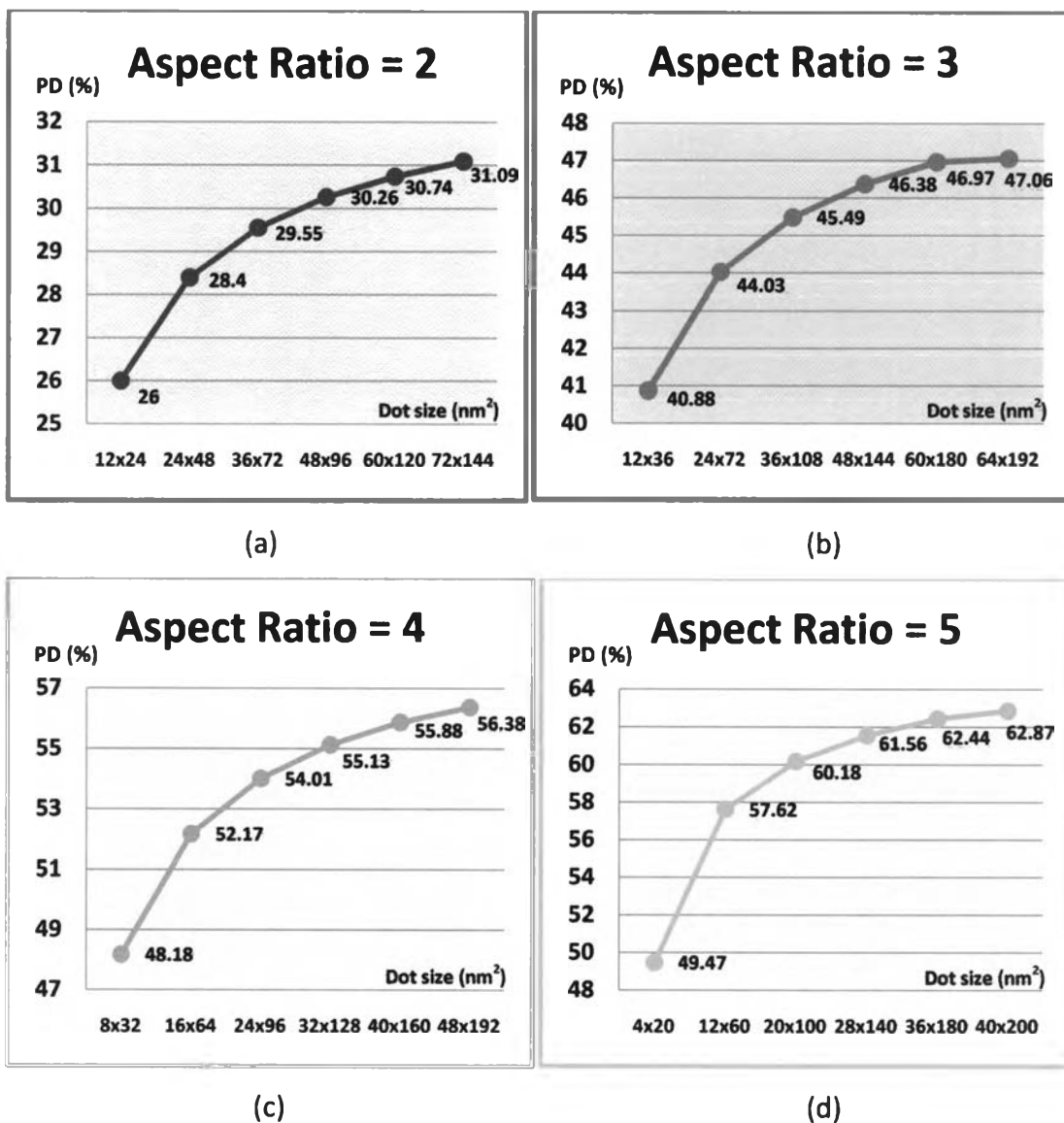


**Figure 3.9** The polarization degree of elongated QDs with different aspect ratio of (a) 2, (b) 3, (c) 4, and (d) 5, respectively.

The polarization degree values of QDs with other various sizes and aspect ratios were also calculated by using the parameters shown in **Table 3.4** separated into four groups. Each group consists of elongated QDs with aspect ratio varied from 2 to 7. The result is shown in **Figure 3.10** that agrees with the previous results.

**Table 3.4:** Comparison of polarization degree of QDs with various sizes and aspect ratios.

Aspect Ratio	Group 1		Group 2		Group 3		Group 4	
	Size (nm <sup>2</sup> )	PD (%)	Size (nm <sup>2</sup> )	PD (%)	Size (nm <sup>2</sup> )	PD (%)	Size (nm <sup>2</sup> )	PD (%)
2	8x16	24.28	12x24	26	16x32	27.06	24x48	28.4
3	8x24	38.59	12x36	40.88	16x48	42.29	24x72	44.03
4	8x32	48.18	12x48	50.66	16x64	52.17	24x96	54.01
5	8x40	55.12	12x60	57.62	16x80	59.13	24x120	60.96
6	8x48	60.38	12x72	62.84	16x96	64.31	24x144	66.07
7	8x56	64.52	12x84	66.9	16x112	68.25	24x168	70

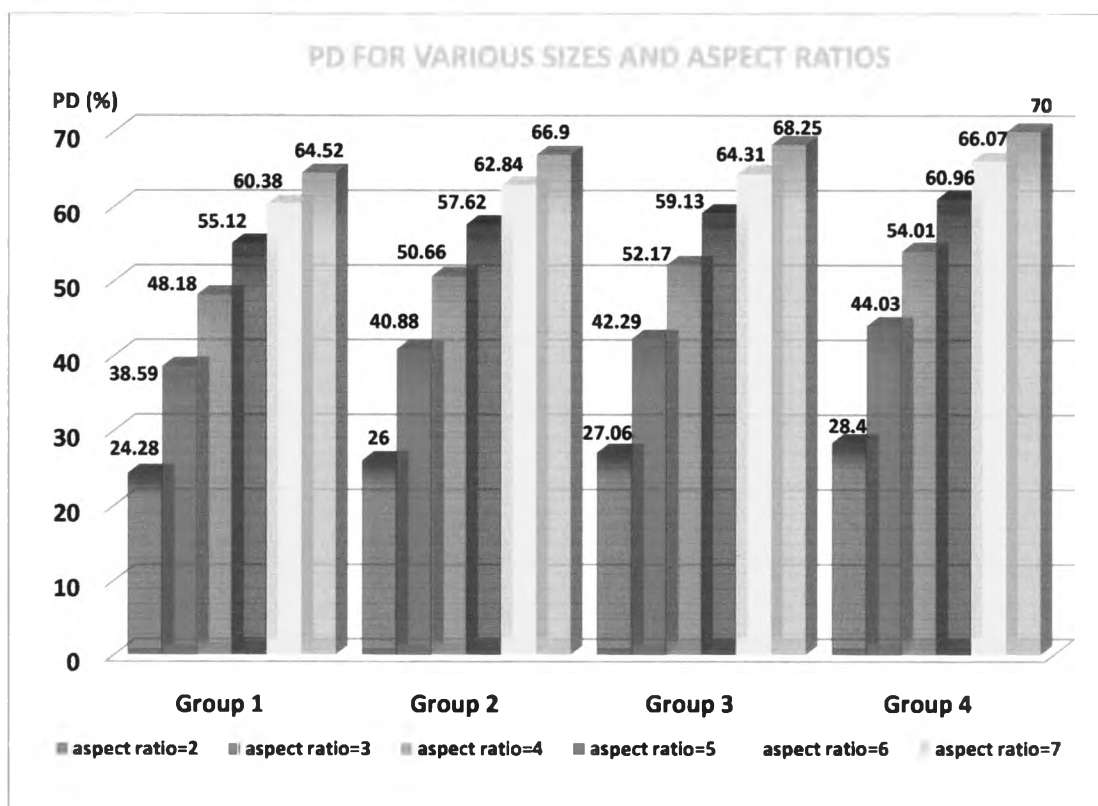


**Figure 3.10** Bar chart for PD values of QDs with various sizes and aspect ratios.

### 3.1.4.2.2 Aligned quantum dots

In this section, we represent the calculation of polarization degree for linearly aligned QDs extended from the former case. The two-dimensional aligned QDs system was modeled, as depicted in **Figure 3.11**. The identically rectangular QDs whose width and size are  $n$  and  $a$  nm, respectively. Here,  $d$  is the spatial separation of QDs that is the same range for all adjacent QDs. It was observed that there were some barriers between QDs and needed to be taken into account in the calculation which was more complicated. The separation of QDs by the barrier thickness strongly affects the “overlap integral”  $\Gamma$ , which measures the amount of total coupling both interdot overlapping (between electron-electron wavefunctions and hole-hole wavefunctions in the adjacent QDs) and intradot overlapping (between electron and hole wavefunctions in the same QD or refers as Coulomb interaction) of carriers, and is defined as:

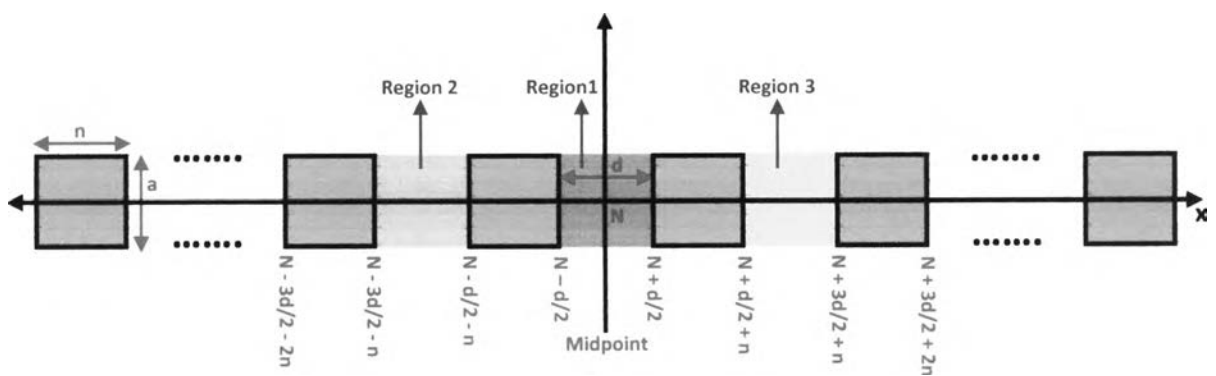


**Figure 3.11** Schematic diagram of two-dimensional aligned QD system. Each QD size is  $n \times a$  nm<sup>2</sup> and interdot spacing  $d$  nm.

$$\Gamma = \frac{Mid + Left + Right}{\int_{-\frac{a}{2}}^{\frac{a}{2}} \int_{-\frac{d}{2}}^{\frac{d}{2}} dx dy} \quad (3.9)$$

$$Mid = \sum_{i=1}^K \int_{-\frac{a}{2}}^{\frac{a}{2}} \int_{-\frac{d}{2}}^{\frac{d}{2}} \left\{ \psi_e(x, y) \cdot \psi_e^*(x, y) + \psi_h(x, y) \cdot \psi_h^*(x, y) - 2[\psi_e(x, y) \cdot \psi_h^*(x, y)] \right\} dx dy \quad (3.10)$$

$$Left = \sum_{i=1}^K \int_{-\frac{a}{2}}^{\frac{a}{2}} \int_{N-(2i-1)d/2-0}^{N-(2i-1)d/2+0} \left\{ \psi_e(x, y) \cdot \psi_e^*(x, y) + \psi_h(x, y) \cdot \psi_h^*(x, y) - 2[\psi_e(x, y) \cdot \psi_h^*(x, y)] \right\} dx dy \quad (3.11)$$

$$Right = \sum_{i=1}^K \int_{-\frac{a}{2}}^{\frac{a}{2}} \int_{N+(2i-1)d/2+0}^{N+(2i-1)d/2+0} \left\{ \psi_e(x, y) \cdot \psi_e^*(x, y) + \psi_h(x, y) \cdot \psi_h^*(x, y) - 2[\psi_e(x, y) \cdot \psi_h^*(x, y)] \right\} dx dy \quad (3.12)$$

where  $\psi_e$  and  $\psi_h$  are the ground-state wavefunction of electron and hole, respectively.  $K = (\text{half number of QDs}) - 1$ . *Mid*, *Left*, and *Right* are overlapping region in the central, left side, and the right side of aligned QDs system, respectively. By summation of integrating the dot product of electron-electron, hole-hole, and electron-hole wavefunctions overall coupling space, the overlap integral of aligned QDs system was obtained. Note that since the dimension of each overlapping region was the same, therefore the normalization factor in Eq. (3.9) was the same in all overlapping regions. In other words, the normalization factor in all overlapping regions can be calculated by using the formula  $\int_{-\frac{a}{2}}^{\frac{a}{2}} \int_{-\frac{d}{2}}^{\frac{d}{2}} dx dy = d \times a \text{ nm}^2$  or the area of

barrier region for each adjacent QDs. Additionally, we neglect the cross-coupling effect [223] since it is very small compared with the coupling effect from the two neighboring QDs. For example, if the number of QDs equal to 4,  $K = (4/2) - 1 = 1$ . The *Mid*, *Left*, and *Right* are calculated by overlapping of wavefunctions in the region 1, 2, and 3, as shown in Figure 3.11, respectively.

Finally, the total polarization degree of aligned QDs system may be calculated by

$$PD_{total} = \Gamma \times \left| \frac{I_x - I_y}{I_x + I_y} \right| = \Gamma \times RawPD \quad (3.13)$$

It was observed that Eq. (3.13) was modified from Eq. (3.8) by the multiplicative factor  $\Gamma$ , which is important factor to be taken into account for any coupled QDs systems. Furthermore, *RawPD* means the original polarization degree before combining the factor  $\Gamma$ , result in the total polarization degree  $PD_{total}$  of the aligned QDs system.

### Increase of polarization degree with number of QDs

Next, we will examine the effect of number of QDs on the polarization degree. The even number of QDs was increased in the x direction which was varied from two to twelve QDs, while for the y direction, only one QD was maintained. In this case, each QD size was maintained at  $12 \times 12 \text{ nm}^2$  and the thickness of barrier (spacing between aligned QDs) was fixed at 2 nm. The degree of linear polarization of the aligned QDs system was calculated

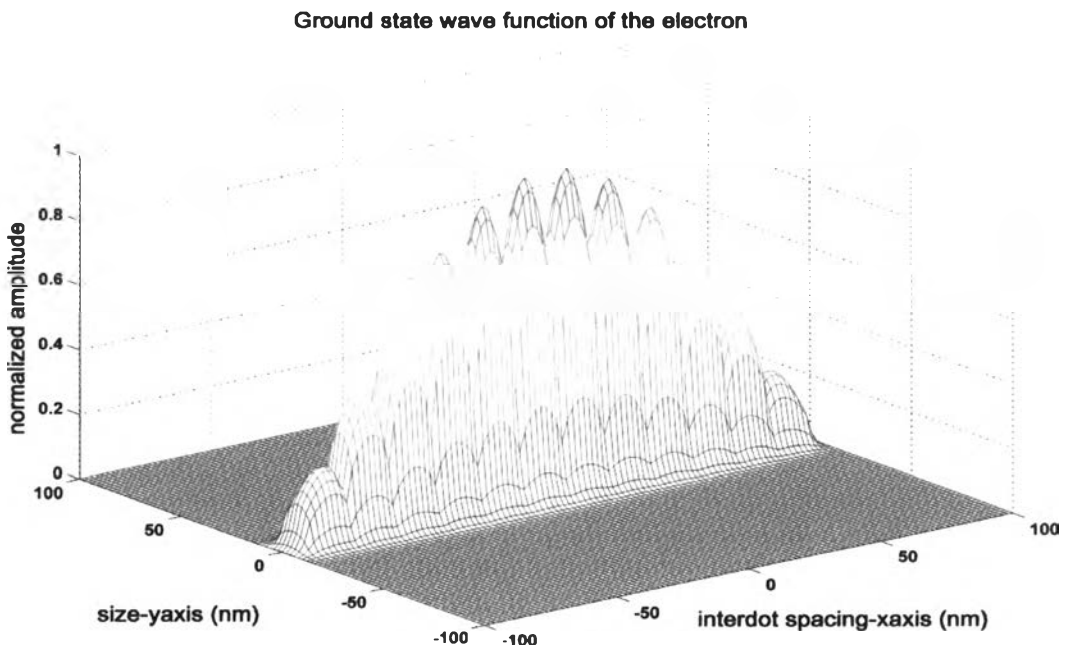


**Figure 3.12** The ground-state electron wavefunction of twelve QDs (highest number of QDs that can be calculated), each of size  $12 \times 12 \text{ nm}^2$  with interdot spacing of 12 nm.

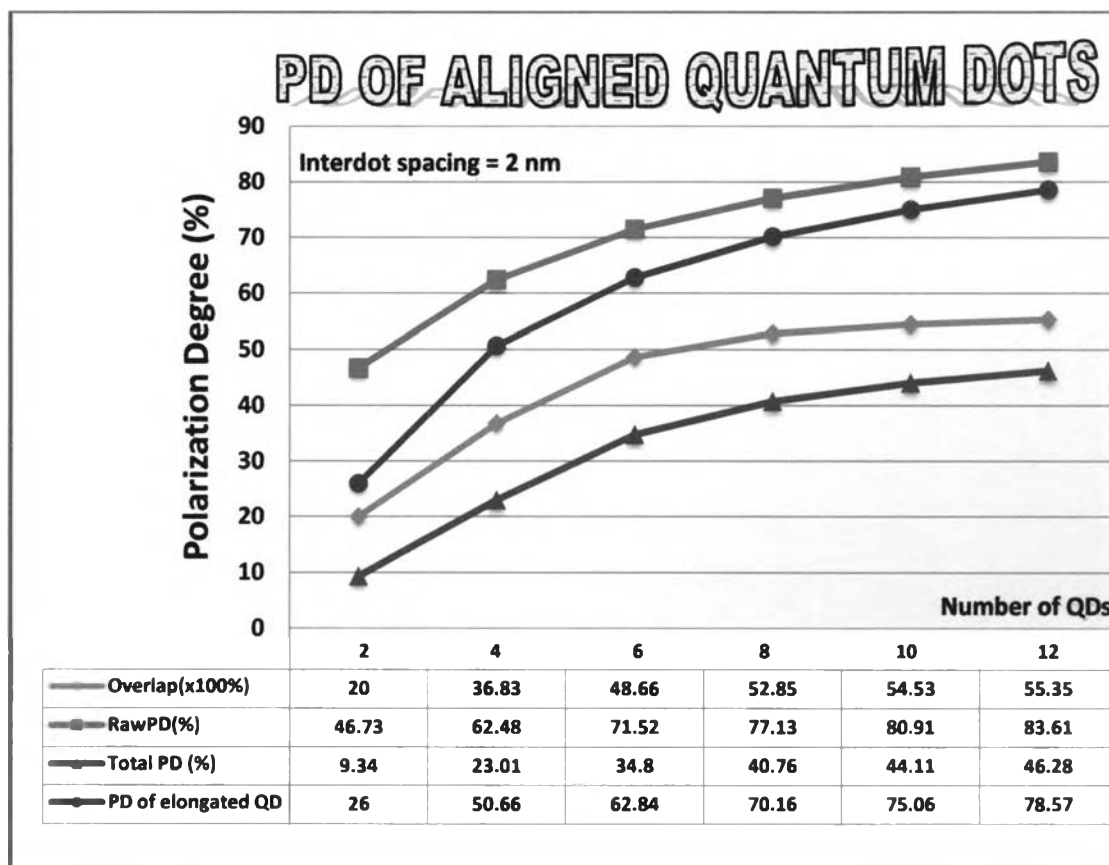


**Figure 3.13** Comparison of overlap integral (pink line), RawPD (red line), and total PD (blue line) vs. the number of QDs aligned in the x direction. The dot size was maintained at  $12 \times 12 \text{ nm}^2$  (isotropic shape), and the interdot spacing between adjacent QDs was fixed at 2 nm. The number of QDs increased in the x direction. The PD of elongated single QD (violet line) was also plotted for comparison.

by using Eq. (3.13). It was found that when the number of QDs increased, the total polarization degree also increased, as shown in Figure 3.13, and slowly increased when reached to the higher number of QDs. The overlap integral and RawPD values also show a similar trend, compared with the total PD. Note that the overlap integral were multiplied by 100 in order to plot in the same scale with polarization degree values (generally, the overlap integral is between 0 and 1). Explanation of the results can be interpreted both energy splitting and QDs coupling. The energy splitting of any coupled QD system is significant in the direction of the dot alignment [207, 224].

As the number of dots increases, the amount of energy splitting also increases. In two-dimensional system, if the QDs align, for example, in the  $x$  direction, then the splitting of energy levels is significant in the  $x$  direction, there is virtually not much energy splitting in the  $y$  direction. The major contribution to the optical transition is the  $x$  component of the wavefunctions. Consequently, significant energy splitting in the  $x$  direction implies dominant linear polarization in the  $x$  direction.

In the view of QDs coupling mechanism, when the QDs interact with each other, they form a coupled system. As the number of dots increases, the overlapping region also increases corresponding to strongly mutual coupling from the additional carriers. This becomes important for QDs coupling, since the coupling between the states of QDs is determined by the overlap of corresponding wavefunctions. Therefore, the QDs coupling exhibits a large optical intensity spreading in the direction of aligned QDs and becomes sensitive to the polarization with the same direction too.

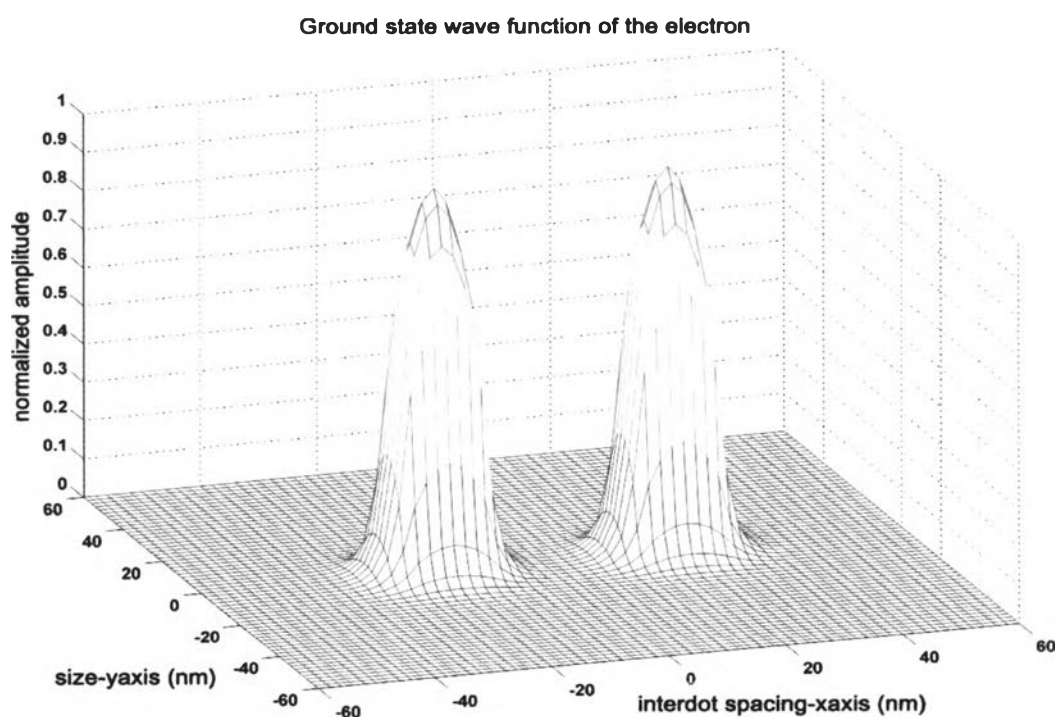
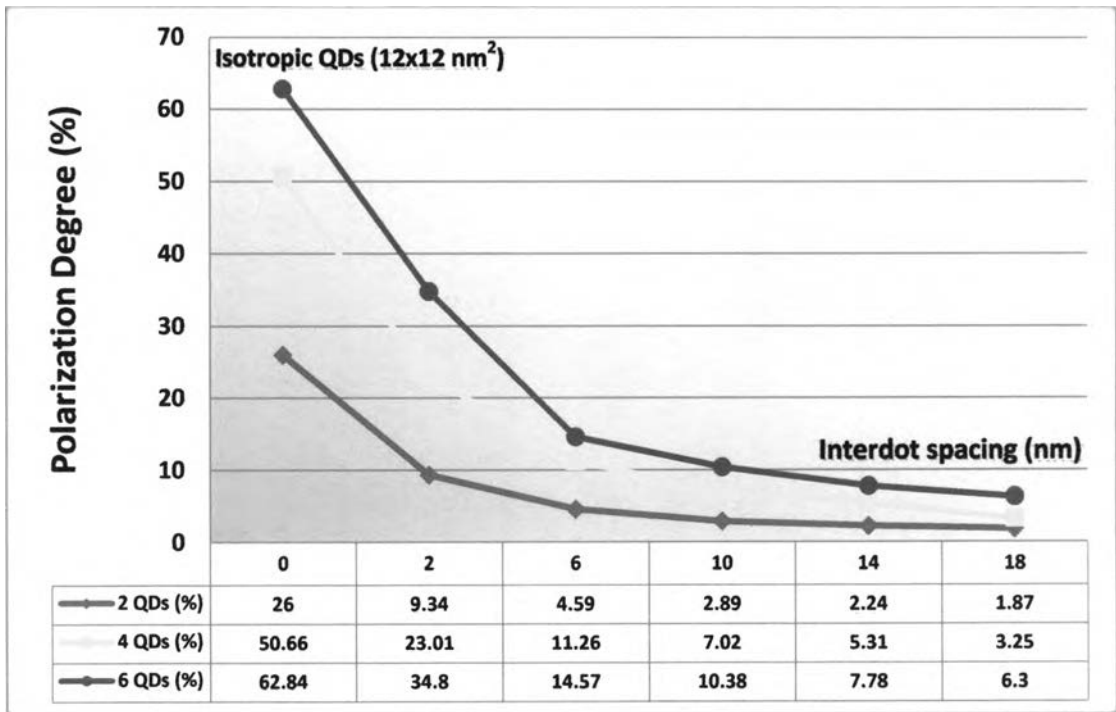
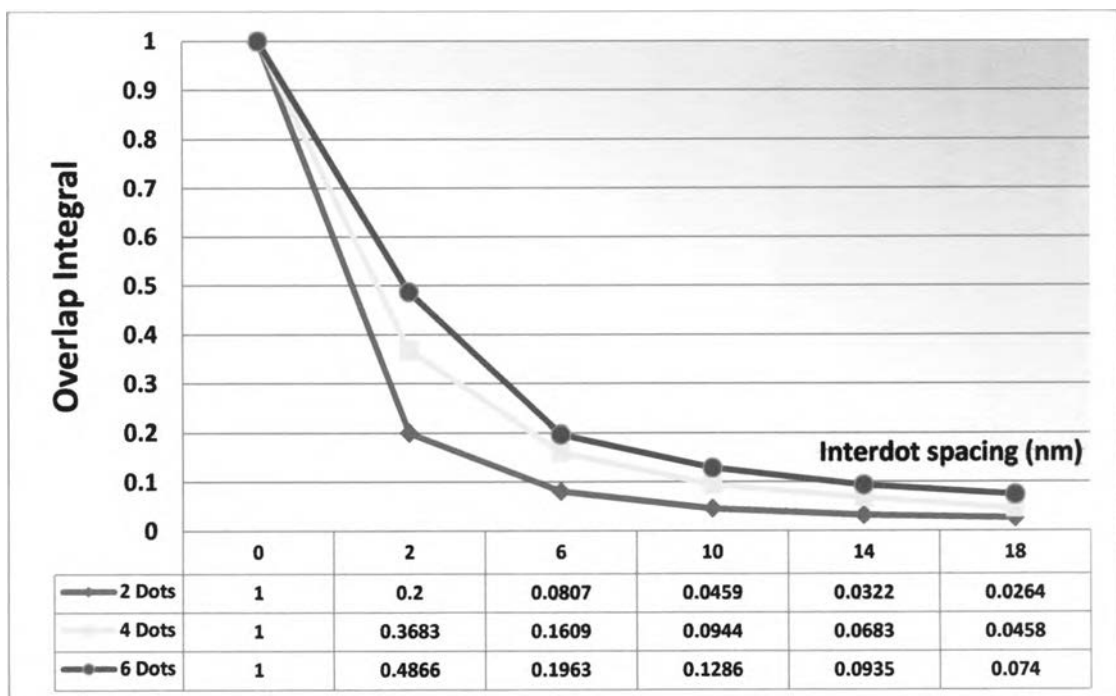


**Figure 3.14** The ground-state electron wavefunction of binary QDs, each of size  $12 \times 12 \text{ nm}^2$  with interdot spacing of 22 nm.





(a)



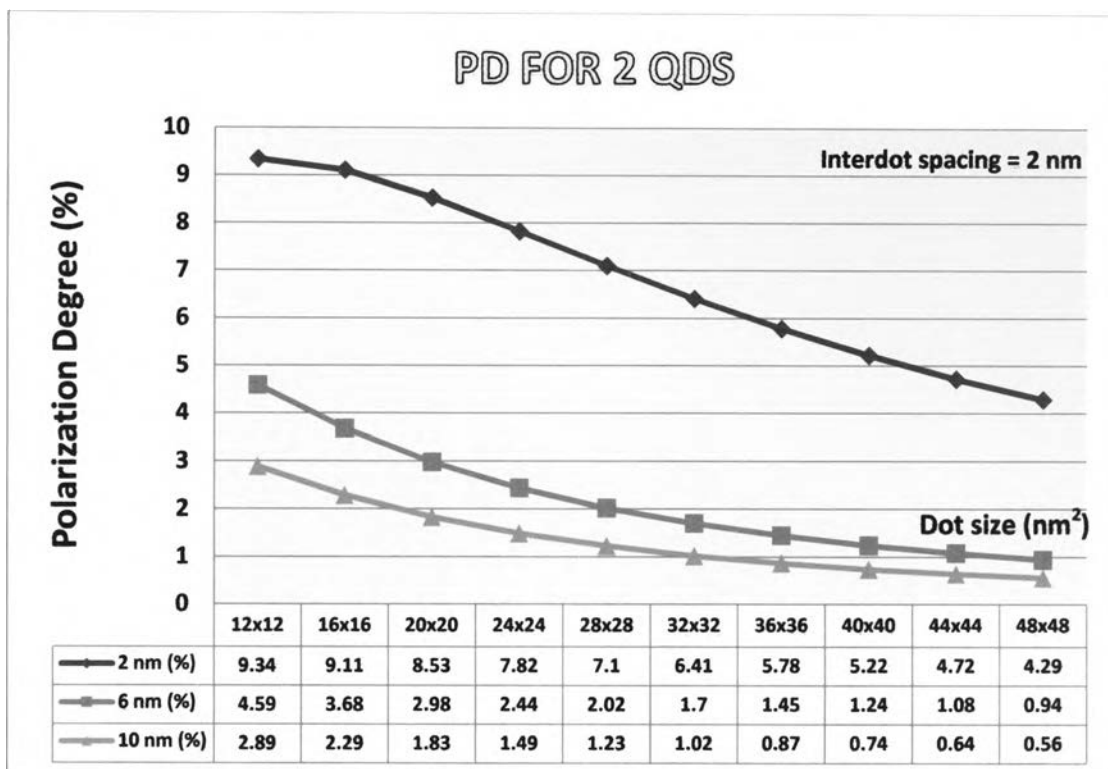
(b)

**Figure 3.15** (a) The polarization degree of 2, 4 and 6 QDs, and (b) the overlap integral of aligned QDs vs. their interdot spacing (dot size was fixed at  $12 \times 12 \text{ nm}^2$  and the interdot spacing was varied from 0 to 18 nm).

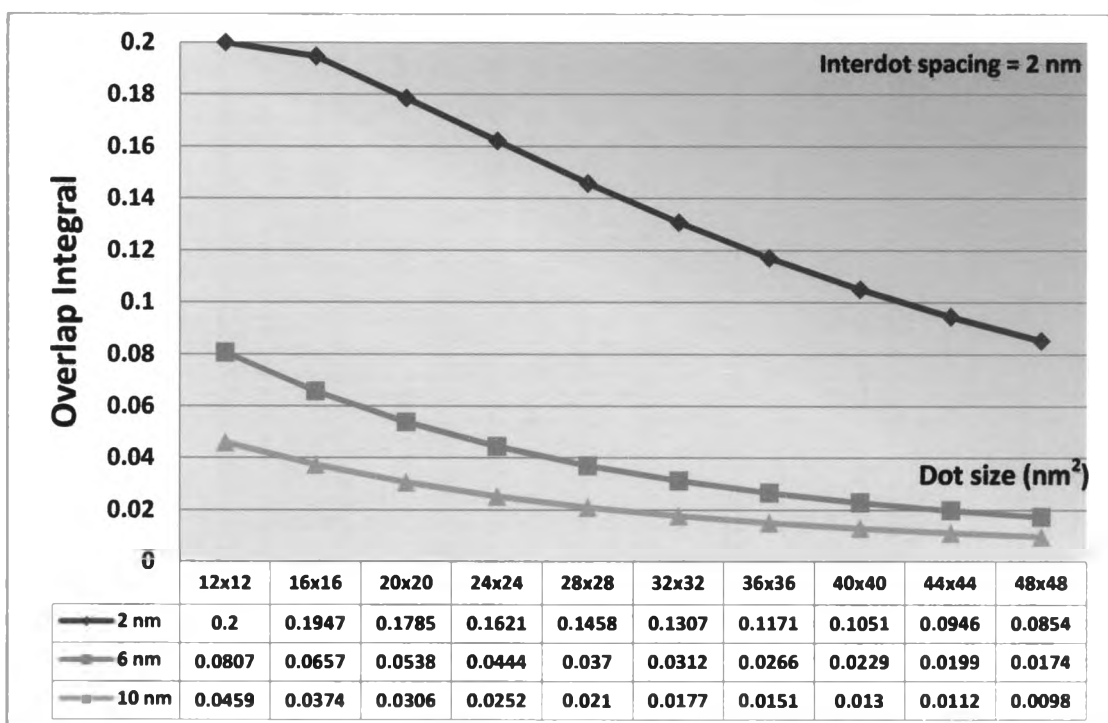
### Variation of polarization degree with spacing between the QDs

One of the considerable cases of aligned QDs behavior is to understand about the polarization degree of for different interdot distances. **Figure 3.15 (a)** illustrates the polarization degree of two, four, and six aligned QDs for various interdot distances varied from 0 to 18 nm, each QD is isotropic with the dimension of  $12 \times 12 \text{ nm}^2$ . The thickness of the barrier between the QDs in their alignment direction plays important role to determine the polarization degree of them. The polarization degree tends to decrease when the spatial separation between the QDs increases. For the overlap integral of aligned QDs, the results shows us that the wavefunction coupling also strongly depends on the mutual distance between the QDs, seen in **Figure 3.15 (b)**. The tendency of the overlap integral, when varying the interdot spacing is inversely proportional to the increasing distance which is similar to exponential variation. Increasing the interdot distance, the ground levels of QDs should expect a very small coupling. At the large distance, for example, 22 nm, the electron wavefunction is shown in **Figure 3.14**. The wavefunction decouples and no coupling region appears indicating the all energy levels are nearly degenerate state when the QDs are far enough from each other. These imply that overlap integral becomes very sensitive to the spacing between QDs.

According to the results mentioned above, we see that the approach for increasing the degree of polarization is decreasing the interdot spacing between QDs which is close enough so that coupling between them manifests. When the thickness of the barrier is smallest, the highest PD is obtained and the band structure of the system may be seen as the single longer potential well, as previously discussed in **section 3.1.4.1**. In **Figure 3.13**, we see that all of the polarization degree values of elongated QDs (violet line) are greater than the polarization degree in case the distance between QDs is 2 nm (pink line). This may be estimated that each case of polarization degree of elongated QD is approximately equivalent to the highest PD of aligned QDs which the distance between them is zero (completely attachment or

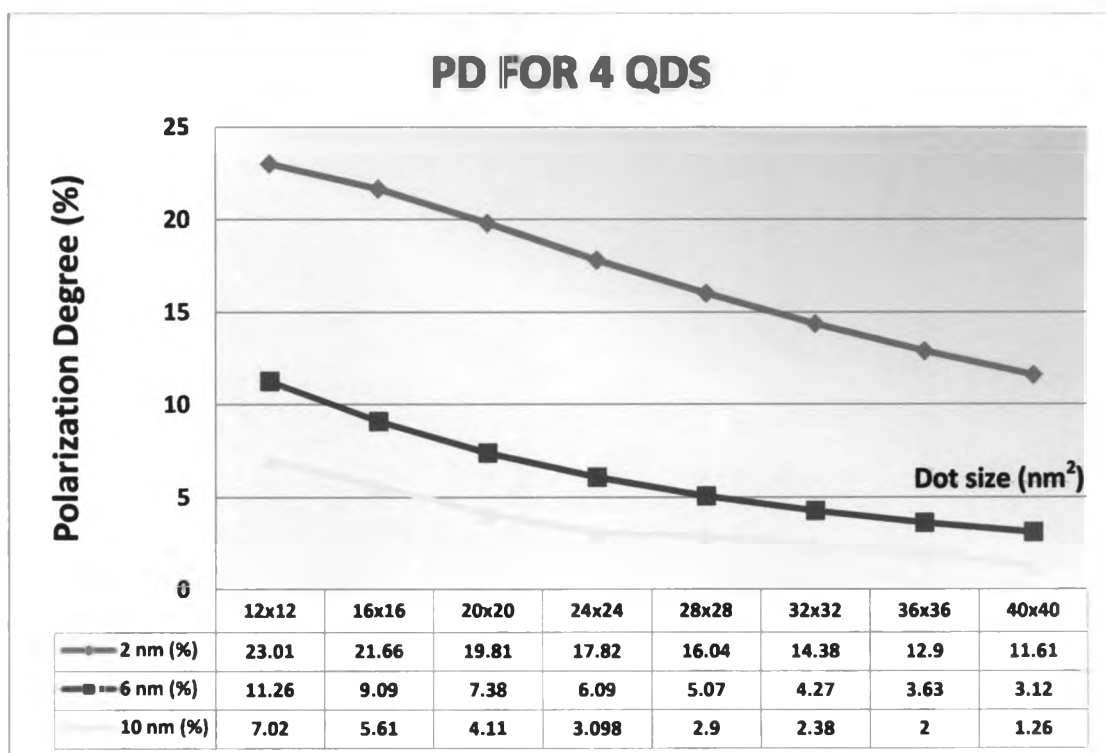


(a)

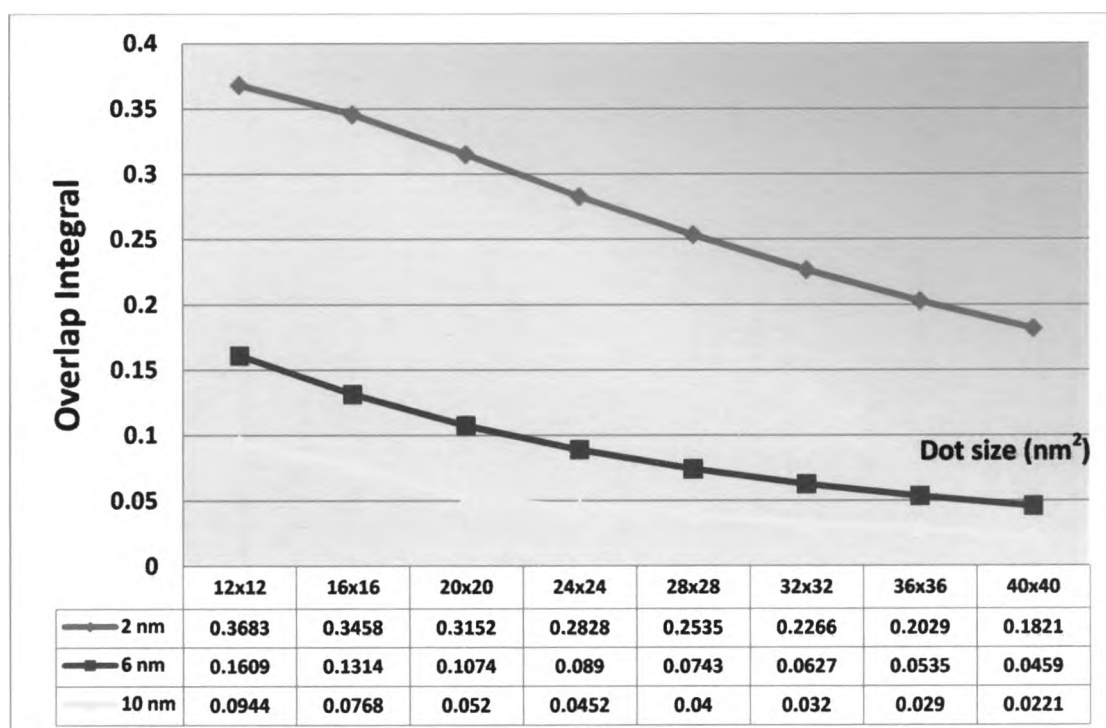


(b)

**Figure 3.16** (a) The polarization degree of two isotropic QDs, and (b) the overlap integral of aligned QDs with various dot sizes varied from  $12 \times 12 \text{ nm}^2$  to  $48 \times 48 \text{ nm}^2$ . The interdot spacing was also plotted at 2, 6, and 10 nm, respectively.



(a)



(b)

**Figure 3.17** (a) The polarization degree of two isotropic QDs, and (b) the overlap integral of aligned QDs with various dot sizes varied from  $12 \times 12 \text{ nm}^2$  to  $40 \times 40 \text{ nm}^2$ . The interdot spacing was also plotted at 2, 6, and 10 nm, respectively.

overlap integral = 1). In practice, it is impossible to grow the large elongated QD structure since it is high probably to form an amount of long strips structure on the substrate. Nevertheless, we have an option by growing the aligned QDs instead and controlling the interdot spacing to become as close as possible.

### **Influence of increasing the QD size on the linear polarization degree**

The effect of dot sizes on the polarization degree was also investigated by increasing the size altogether both x and y direction. **Figure 3.16 (a)** shows the polarization degree of two isotropic QDs, sizes varied from  $12 \times 12 \text{ nm}^2$  to  $48 \times 48 \text{ nm}^2$ . The data clearly shows the decreasing of PD while increasing the size of the dots and the overlap integral also shows a similar trend, as seen in **Figure 3.16 (b)**. In addition, the polarization degree will highly decreases when increases the distance between QDs. The PD and overlap integral results for four aligned QDs (see **Figure 3.17**) were the same as in the case of two aligned QDs. Though, enlargement of QD size produces a large carrier wavefunctions, the dimension of each quantum well is also large enough to confine their wavefunctions that can decrease the probability to find the partial wavefunctions outside quantum wells. Hence, with increasing the dot size, the ground-state wavefunctions of carriers in aligned QDs should expect very small coupling and the PD then should decrease, corresponding to [224].

### 3.2 CALCULATION OF TWO-DIMENSIONAL ELECTRIC FIELD SYSTEM

Following to the topic, this section will be discussed the most important calculation part, which is directly related to the thesis work. The simulation of two-dimensional electric field system is demonstrated. Many research have determined the electric field as a specific value, so the electric field was applied in one direction. As a result, both the conduction band and the valence band in QDs structure was linearly tilted down to the electric field direction. Expansion the electric field modeling to become more flexible, two-dimensional electric field system was produced.

The intention of this point is to improve an accuracy of the system from one-dimensional model. The in-plane electric field system allows for adjusting the applied field which may occurred of both directions (i.e.,  $x$  and  $y$ ) in the plane. Because electric field is a vector quantity, the total electric field is the component of electric field in  $x$  and  $y$  direction which can define the scalar values of them for the different cases. If electric field is applied only in the  $x$  direction, the total electric field vector is shown in the  $x$  direction. When electric field is applied in both  $x$  and  $y$  direction, the total electric field manifests in the direction making arbitrary angle on the plane, corresponding to their scalar values. This is capable for fine-tuning the direction of electric field to point in the required direction.

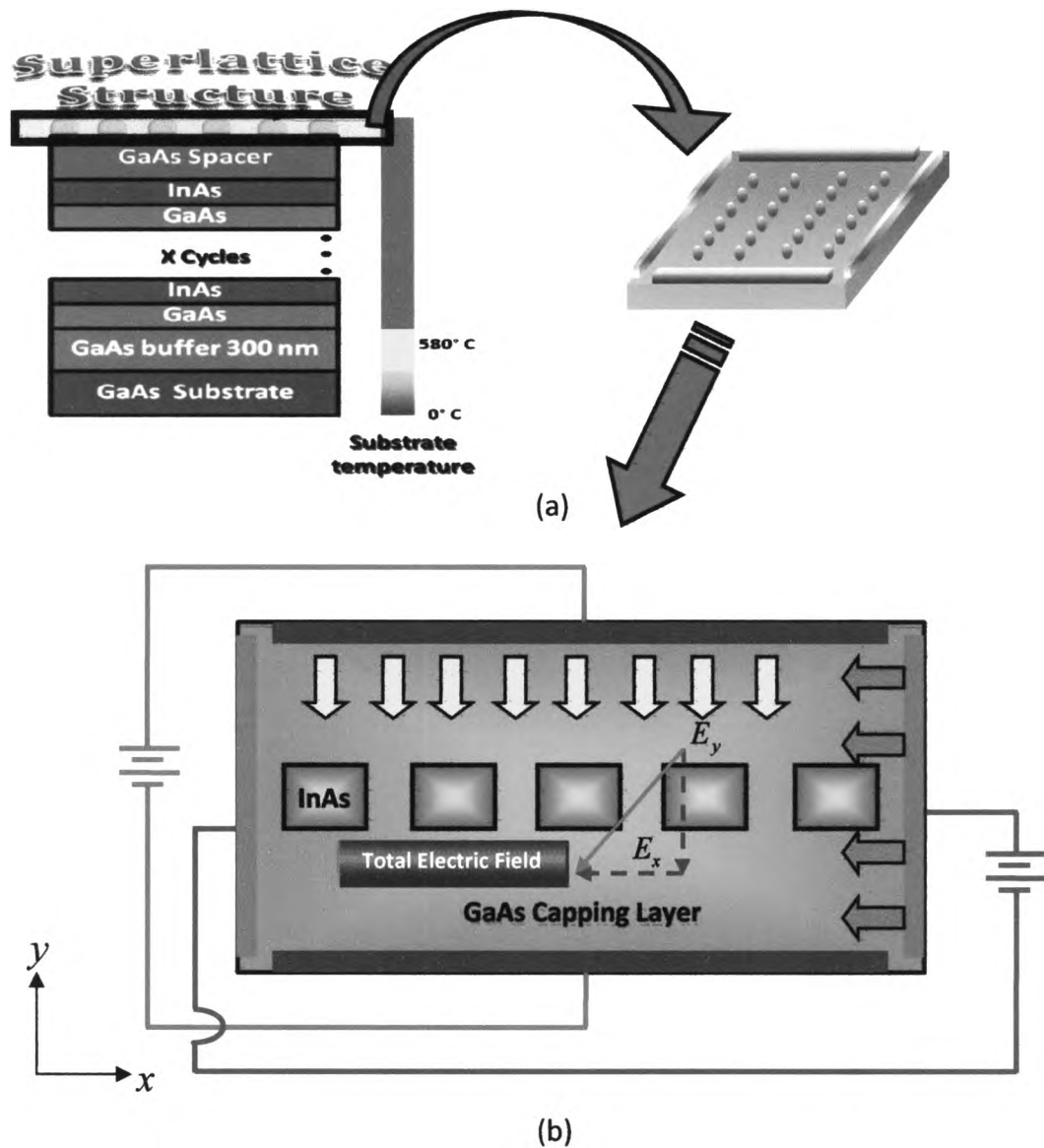


**Figure 3.18** Schematic diagram of (a) self-aligned QDs structure and (b) the configuration of two-dimensional electric field system.

### 3.2.1 Mathematical Model

The schematic diagram of self-aligned QDs was depicted in **Figure 3.18 (a)**. Since the calculation of electric field model was added to the previous model, QDs structure was considered to InAs/GaAs QDs structure, same as discussed in **section 3.1**. The configuration of two-dimensional electric field system was shown in **Figure**

**3.18 (b)**, the InAs/GaAs QDs structure was modeled by rectangular InAs QDs were aligned themselves on the horizontal direction ( $x$ ) and embedded in rectangular GaAs capping layer. Two pairs of electrode were attached on the GaAs surface both horizontal ( $x$ ) and vertical direction ( $y$ ) which were perpendicular to the growth direction. It was assumed that the thickness of all electrodes were neglected, so the electric field component was appeared only with paralleling along the GaAs surface. Moreover, the voltage value in each electrode was constant through the width of electrode for simplicity in calculation.

It was observed that the structure in this case was related with the electrostatics problem with boundary conditions. Because the problem was two-dimensional area, it is not easy to calculate by using analytical method, especially by superposition. The reason is not only there are more elements which are not a blank area, but also induce the additional internal boundary conditions, causing the problem with more complexity. Therefore, numerical calculation regime will be used again to manage in this situation. The solution of this electric field structure will be explained by means of numerical approach in the next topic.

### **3.2.2 Simulation of Two-Dimensional Electric Field System by Numerical Approach**

Many problems in electrostatics involve boundaries that do not coincide with the coordinate surfaces of rectangular, cylindrical, or spherical coordinate systems. Analytical methods may not be useful in these cases, and numerical methods must be employed. A powerful method for solving Poisson's or Laplace's equation subject to conditions on boundary surfaces of arbitrary shapes is the FDM method, which makes use of finite difference approximations. Following the electric field model mentioned in this thesis work is within the scope of **Laplace's equation**, so the FDM method can be used to investigate the electric field value absolutely [225]. The FDM method may be summarized as follows:



- The partial differential equation  $-\nabla^2\Phi = -\frac{\rho_v}{\epsilon}$  is replaced by its finite difference approximation on a regularly-spaced grid of points covering the region of interest. This approximation expresses the potential at grid points interior to the region in terms of weighted averages of potential at neighboring points of the grid. Potential at grid points on the region's semiconductor boundaries are fixed by the boundary conditions.

- The system of finite difference equations constitutes a linear system that may be solved either by standard methods, such as Gaussian elimination, or by iterative methods.

#### Finite Difference – Explicit Method

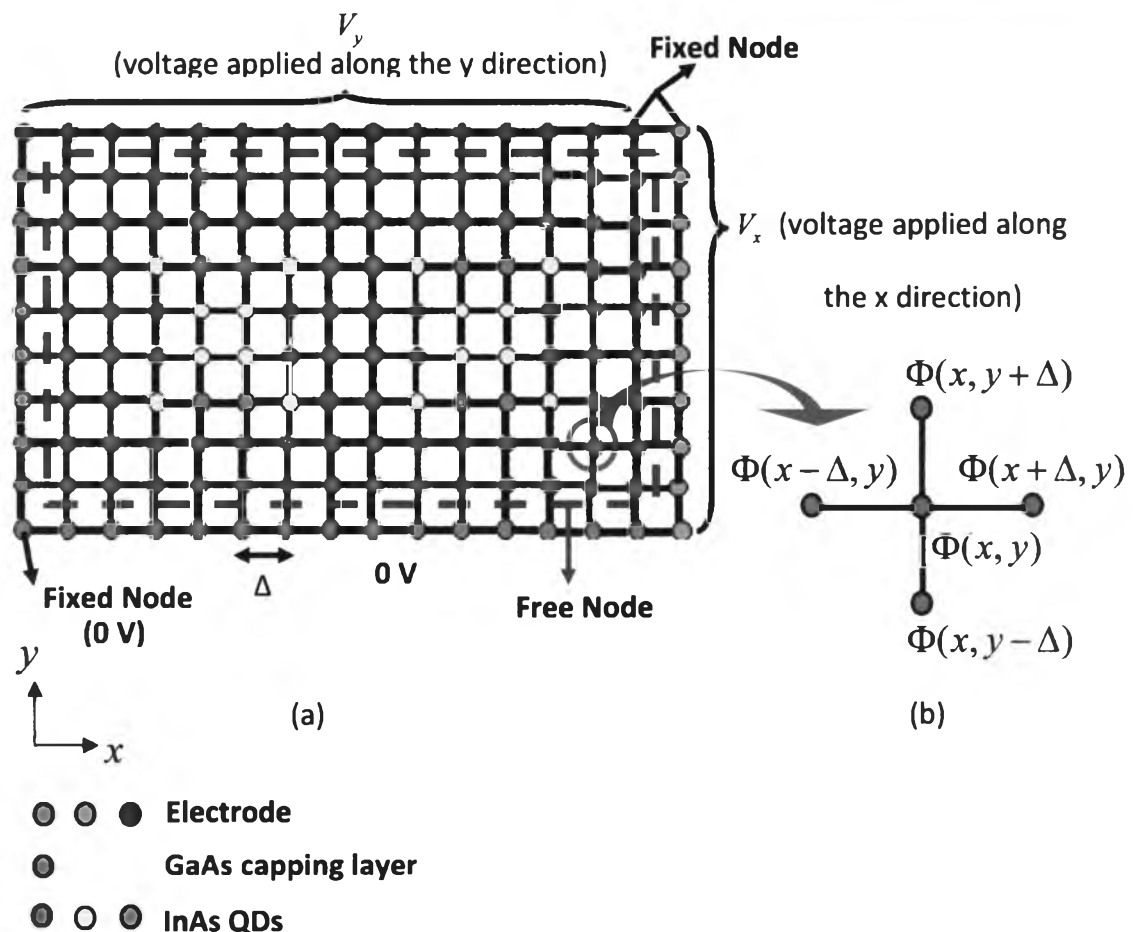


**Figure 3.19** Geometry of a rectangular grid used to approximate a 2D electrostatics problem, and (b) expansion view of the “computational molecule” used to solve the finite difference problem.

In two-dimensional electric field system, first, the overall area must be mapped to the group of nodes on the rectangular grid with spacing  $\Delta$  on each node illustrated in **Figure 3.19**. The GaAs capping layer region is the component of red nodes. The InAs QDs regions are the component of yellow, pink, and violet nodes. The electrode regions are the component of blue, brown, and green nodes. Each node is the voltage value or solution region  $\Phi(x,y)$  that can be classified in three groups:

- Fixed node: a node which is specified a voltage value initially or fixed boundary condition (blue, brown, and green nodes).
- Free node: a node which its voltage (or potential) value is unknown and depended on the surrounding nodes with the same material region (red and yellow nodes).
- Free node with interface area: a node which is located between two different material regions (pink and violet nodes).

Consider finding a solution for the potential  $\Phi(x,y)$  in a two-dimensional, charge-free ( $\rho_v = 0$ ) region bounded by electrodes on which the potential is specified. Hence, Poisson's equation reduces to Laplace's equation,

$$\nabla^2\Phi = \frac{\partial^2\Phi}{\partial x^2} + \frac{\partial^2\Phi}{\partial y^2} = 0 \quad (3.14)$$

Since the values on the boundary are known, the potential is to be estimated at all **interior node** points of the grid. From **Eq. (3.14)**, using finite difference approximations to the derivatives that appear there, the second order derivatives in Laplace's equation are approximated by "**differences of difference**" approximations. That is, the second derivatives are approximated by finite (central) difference approximations of first derivatives,

$$\frac{\partial^2 \Phi(x, y)}{\partial x^2} \approx \frac{\frac{\partial \Phi\left(x + \frac{\Delta}{2}, y\right)}{\partial x} - \frac{\partial \Phi\left(x - \frac{\Delta}{2}, y\right)}{\partial x}}{\Delta} \quad (3.15)$$

which are in turn also approximated as finite differences,

$$\frac{\partial \Phi\left(x + \frac{\Delta}{2}, y\right)}{\partial x} \approx \frac{\Phi(x + \Delta, y) - \Phi(x, y)}{\Delta} \quad (3.16)$$

$$\frac{\partial \Phi\left(x - \frac{\Delta}{2}, y\right)}{\partial x} \approx \frac{\Phi(x, y) - \Phi(x - \Delta, y)}{\Delta}$$

Combining the two approximations (2) and (3) yields

$$\frac{\partial^2 \Phi(x, y)}{\partial x^2} \approx \frac{\Phi(x + \Delta, y) - 2\Phi(x, y) + \Phi(x - \Delta, y)}{\Delta^2} \quad (3.17)$$

Similarly, we have

$$\frac{\partial^2 \Phi(x, y)}{\partial y^2} \approx \frac{\Phi(x, y + \Delta) - 2\Phi(x, y) + \Phi(x, y - \Delta)}{\Delta^2} \quad (3.18)$$

and hence the finite difference approximation to Laplace's equation becomes

$$\begin{aligned} & \frac{\partial^2 \Phi(x, y)}{\partial x^2} + \frac{\partial^2 \Phi(x, y)}{\partial y^2} \\ & \approx \frac{\Phi(x + \Delta, y) - 2\Phi(x, y) + \Phi(x, y + \Delta) + \Phi(x - \Delta, y) + \Phi(x, y - \Delta) - 4\Phi(x, y)}{\Delta^2} \end{aligned} \quad (3.19)$$

Solving for  $\Phi(x, y)$ , it is shown that  $\Phi(x, y)$  at any node is simply the **average of its four nearest neighbors** which was shown in **Figure 3.19 (b)** and its value is:

$$\Phi(x, y) = \frac{\Phi(x + \Delta, y) + \Phi(x, y + \Delta) + \Phi(x - \Delta, y) + \Phi(x, y - \Delta)}{4} \quad (3.20)$$

By applying **Eq. (3.20)** at every interior node, the system of linear equations can be generated. To solve the problem, iterative procedure was given by assigning arbitrary initial values (0, for example, is a possible choice), and then applying the averaging condition of **Eq. (3.20)** to update each interior value successively. After each updating of the interior nodes, the process is repeated until the nodal potential converges. However, this method shows some disadvantages as follows:

- If the arbitrary initial value is assigned far away from the real value, the calculation will take a long time which decreases the calculating performance.
- In case of the large matrix, the number of iterative calculation is rather high. This may cause an error during the calculation.

Fortunately, we had done by creating the special matrix pattern of linear equations set for potential  $\Phi(x, y)$  system. The linear equations were written in form of the linearly matrix equation  $AX = B$ ;  $A$  is the special matrix investigating by inspection method,  $X$  is the matrix of potential  $\Phi(x, y)$  system, and  $B$  is the matrix of manipulated real number. Because all values in the matrix  $A$  was known, the solution of this problem or  $X$  was then solved by inverse matrix approach, that is,  $X = A^{-1}B$ . As a result, the all potential  $\Phi(x, y)$  values were achieved. To describe this process thoroughly, the linearly matrix equation was shown in **Figure 3.20**. This equation was considered to the three components as follows:

## Set of Linear Equations $\Phi(x,y)$ in Matrix Form

$$\underbrace{\begin{bmatrix}
 -4 & 1 & 0 & \dots & 1 & 0 & 0 & \dots & 0 & 0 \\
 1 & -4 & 1 & & 0 & 1 & 0 & & 0 & 0 \\
 0 & 1 & -4 & & 0 & 0 & 1 & & 0 & 0 \\
 \vdots & & & & & & & & & \vdots \\
 1 & 0 & 0 & & -4 & 0 & 0 & & 1 & 0 \\
 0 & 1 & 0 & & 0 & -4 & 1 & & 0 & 1 \\
 0 & 0 & 1 & & 0 & 1 & -4 & & 0 & 0 \\
 \vdots & & & & & & & & & \vdots \\
 0 & 0 & 0 & & 1 & 0 & 0 & & -4 & 1 \\
 0 & 0 & 0 & \dots & 0 & 1 & 0 & \dots & 1 & -4
 \end{bmatrix}}_A \underbrace{\begin{bmatrix} \Phi_{11} \\ \Phi_{12} \\ \Phi_{13} \\ \vdots \\ \Phi_{nn} \end{bmatrix}}_X = \underbrace{\begin{bmatrix} b_{11} \\ b_{12} \\ b_{13} \\ \vdots \\ b_{nn} \end{bmatrix}}_B$$

**Specification Matrix**
**Potential Matrix**
**Boundary Matrix**

**Figure 3.20** Schematic diagram of linearly matrix equation of potential  $\Phi(x,y)$  which stands for all free nodes in the two-dimensional potential system. The specification matrix (matrix  $A$ ) shows a sparse matrix with diagonal form.

**1. Potential  $\Phi(x,y)$  matrix (or matrix  $X$ )** is a  $n^2 \times 1$  matrix (matrix with  $n^2$  rows and one column,  $n$  is the dimension of free nodes) which all matrix elements are potential  $\Phi(x,y)$  of “free nodes” arranged subsequently in the one column (vertically arrangement). In this thesis work, the matrix  $A$  was considered to the **square matrix** for simplicity. Consequently, the matrix of free nodes must be a square matrix with dimension of  $n \times n$ . **Figure 3.21 (a)** depicts the example of the  $6 \times 6$  two-dimensional potential grid points. The potential was applied both  $x$  (green nodes) and  $y$  direction (pink nodes) about 5 and 10 volts, respectively. The red nodes are reference voltage (ground), and the yellow nodes are free nodes. The potential  $\Phi(x,y)$  of free nodes were orderly arranged in the matrix  $X$  to create a  $16 \times 1$  matrix, corresponding to the product of dimension of free nodes ( $4 \times 4$ ).



**2. Specification matrix (or matrix  $A$ )** is a sparse matrix with five non-zero diagonal lines parallel to each other. These lines were separated in three groups as below,

- The main diagonal line (red stripe), or matrix elements  $a_{ij}$  ( $i$  and  $j$  are row and column of matrix position, respectively) with  $i = j$  and their values are  $-4$ . Note that the dimension of matrix  $A$  is equal to  $n^2 \times n^2$

- The diagonal lines which are adjacent to the main diagonal line (yellow stripes), or matrix elements  $a_{ij}$  with  $i = j+1$  and  $j = i+1$ . Their element values are  $1$ , except in the element with  $j$  (in case of  $j = i+1$ ) or  $i$  (in case of  $i = j+1$ ) are divisible by  $n$  (dimension of free nodes). The previous values are replaced by  $0$ . From **Figure 3.21 (b)**, the elements  $a_{ij}$  with  $i = j+1$  and  $j = i+1$  (green stripe) were given the value of  $1$  (i.e.,  $a_{21}, a_{32}, a_{12}, a_{23}$ ), and the conditional elements mentioned above (pink circles) are taken  $0$  value (i.e.,  $a_{54}$  which  $i = 5, j = 4$ , and  $i = j+1$ , because  $j$  is divisible by  $4$  (dimension of free nodes),  $\therefore a_{54} = 0$ ). These diagonal lines are shown by two green stripes.

- The off-diagonal line (blue stripes), or matrix elements  $a_{ij}$  with  $|i - j| = n$ . The element values corresponding to are  $1$ . For instance,  $a_{51}, a_{73}, a_{26}, a_{48}$  in **Figure 3.21 (b)** are the same element value of  $1$  since  $|i - j| = 4$ , following to their dimension. The off-diagonal line is shown by two violet stripes.

Note that the matrix  $A$  is a square matrix with its dimension relates to the square of free nodes's dimension. For example, if dimension of free nodes is  $4 \times 4$ , the dimension of matrix  $A$  is  $(4)^2 \times (4)^2 = 16 \times 16$ . Since matrix  $A$  is a sparse matrix, it can be easy to find the inverse matrix of  $A$  and take it to multiply with the matrix  $B$  for solving the  $\Phi(x, y)$ .

**3. Boundary matrix (or matrix  $B$ )** is  $n^2 \times 1$  matrix (same dimension as matrix  $X$ ) which each matrix element  $b_{ij}$  is related to the potential  $\Phi_{ij}$  of free nodes. The value of  $b_{ij}$  is determined by  $b_{ij} = -(\text{summation of the boundary values which its branches link to the fixed nodes})$ . To illustrate, consider **Figure 3.21 (b)**, showing an applied voltage on the x (green nodes) and y (pink nodes) direction with the value of 5 and 10 volts, respectively (the red nodes are ground nodes). Investigating the value of  $b_{ij}$ , for example,  $b_{14}$ . The value of  $b_{14}$  is given by  $\Phi_{14}$ , because its branches link to both green and pink fixed node,  $b_{14}$  is then equal to  $-(5+10) = -15$  V. The another example is  $b_{24}$ , because its branches link only green pink fixed node, the value of  $b_{24}$  is equal to  $-(10) = -10$  V. For the free node which links only the neighboring free nodes, their values are set to 0.

In the two-dimensional electric field system of the thesis work (**Figure 3.19**), this electrostatics problem is more complicated than the general electrostatics problems. The main reason is appearance of the internal boundary condition related to the difference dielectric constant between two semiconductor materials (InAs and GaAs) [226-227]. **Figure 3.19** shows the two sets of internal boundary condition at the interface between InAs QDs and GaAs capping layer; top and bottom InAs QDs regions (pink nodes) which are parallel to x direction, and lateral InAs QDs regions (violet nodes) which is parallel to y direction. The corner regions of InAs QDs are assumed to free node with occupied the InAs QDs condition (yellow nodes), having a dielectric constant of InAs QDs. The GaAs capping layer region is then specified by free node (red nodes) with the dielectric constant of GaAs material.

For simplicity to understand, the example of  $5 \times 5$  two-dimensional potential system was shown in **Figure 3.22**. The system composes of two materials with different dielectric constant; material A (yellow nodes) with dielectric constant  $\epsilon_1$ , and material B (red nodes) with dielectric constant  $\epsilon_2$ . The dimension of corresponding free nodes is  $3 \times 3$ , and the voltage was applied in the fifth column of all potential nodes (the first column of all nodes was a reference voltage). In many



### Interface between two materials

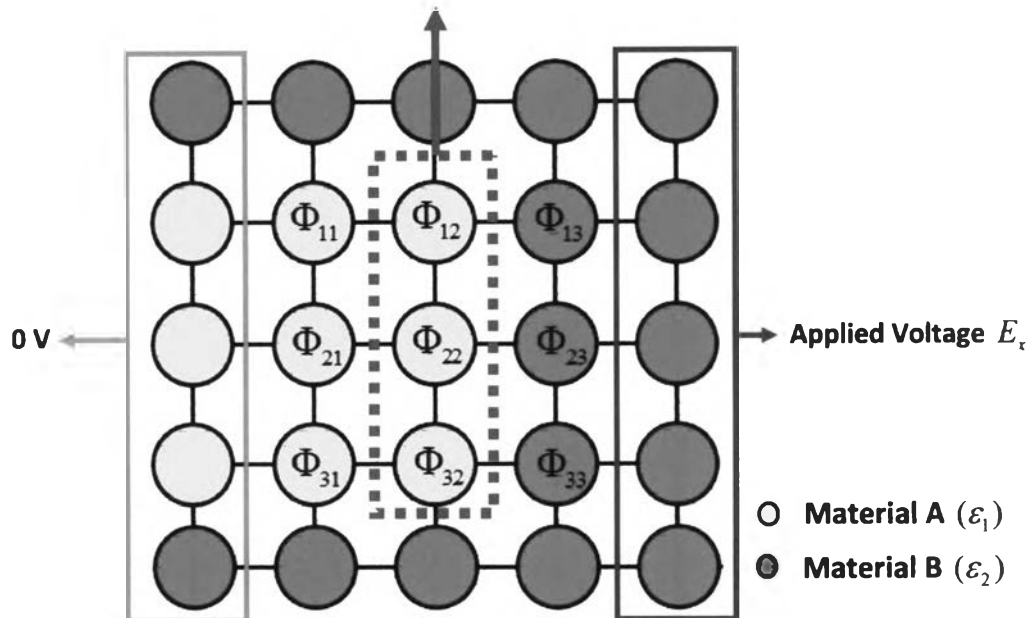


**Figure 3.22** Illustration of  $5 \times 5$  two-dimensional potential system. The electric field is applied along  $x$  direction. The interface between two materials is considered at  $\Phi_{12}$ ,  $\Phi_{22}$ , and  $\Phi_{32}$  (green frame).

electromagnetic problems, the analysis often involves media with different physical properties and requires the knowledge of the relations of the field quantities at an interface between two media. This boundary condition must be satisfied with the continuity of electric flux density  $D$ . The relation between the normal component of the fields at a boundary is “the normal component of  $D$  fields is continuous across an interface when no free charges appear ( $\rho_s = 0$ )”, which leads to the equation [228]

$$D_{1n} = D_{2n} \quad (3.21)$$

or

$$\epsilon_1 E_{1n} = \epsilon_2 E_{2n} \quad (3.22)$$

where  $E_{1n}, E_{2n}$  is the electric field component which normal to the interface in the material A side and material B side, respectively. The electric field was then estimated as

$$E_x = -\frac{\partial\Phi}{\partial x} \approx \frac{\Phi(x+\Delta, y) - \Phi(x, y)}{\Delta}, \quad E_y = -\frac{\partial\Phi}{\partial y} \approx \frac{\Phi(x, y+\Delta) - \Phi(x, y)}{\Delta} \quad (3.23)$$

Consider the interface between two materials (green frame) in **Figure 3.22**. Because electric field was applied along x direction, the horizontal electric field  $E_x$  was concerned. Substituting  $E_x$  from **Eq. (3.23)** into **Eq. (3.22)**, the equation becomes

$$\begin{aligned} \text{at } \Phi_{12}, \quad & \varepsilon_1(\Phi_{12} - \Phi_{11}) = \varepsilon_2(\Phi_{13} - \Phi_{12}) \\ \text{at } \Phi_{22}, \quad & \varepsilon_1(\Phi_{22} - \Phi_{21}) = \varepsilon_2(\Phi_{23} - \Phi_{22}) \\ \text{at } \Phi_{32}, \quad & \varepsilon_1(\Phi_{32} - \Phi_{31}) = \varepsilon_2(\Phi_{33} - \Phi_{32}) \end{aligned} \quad (3.24)$$

Manipulating **Eq. (3.24)** with the simple form, the results was then obtained

$$\begin{aligned} \text{at } \Phi_{12}, \quad & (\varepsilon_1 + \varepsilon_2)\Phi_{12} = \varepsilon_1\Phi_{11} + \varepsilon_2\Phi_{13} \\ \text{at } \Phi_{22}, \quad & (\varepsilon_1 + \varepsilon_2)\Phi_{22} = \varepsilon_1\Phi_{21} + \varepsilon_2\Phi_{23} \\ \text{at } \Phi_{32}, \quad & (\varepsilon_1 + \varepsilon_2)\Phi_{32} = \varepsilon_1\Phi_{31} + \varepsilon_2\Phi_{33} \end{aligned} \quad (3.25)$$

comparison with the **Eq. (3.20)** in the form of summation of surrounding nodes

$$4\Phi(x, y) = \Phi(x+\Delta, y) + \Phi(x, y+\Delta) + \Phi(x-\Delta, y) + \Phi(x, y-\Delta), \text{ given by}$$

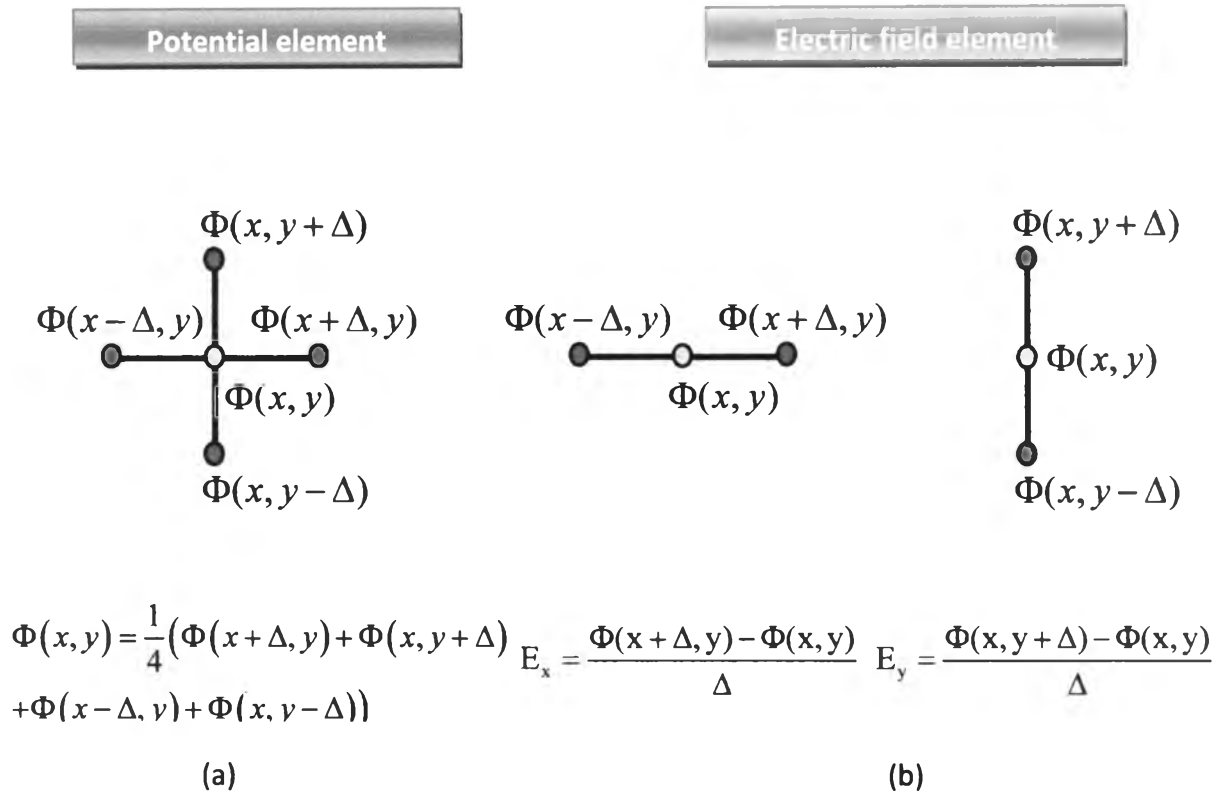
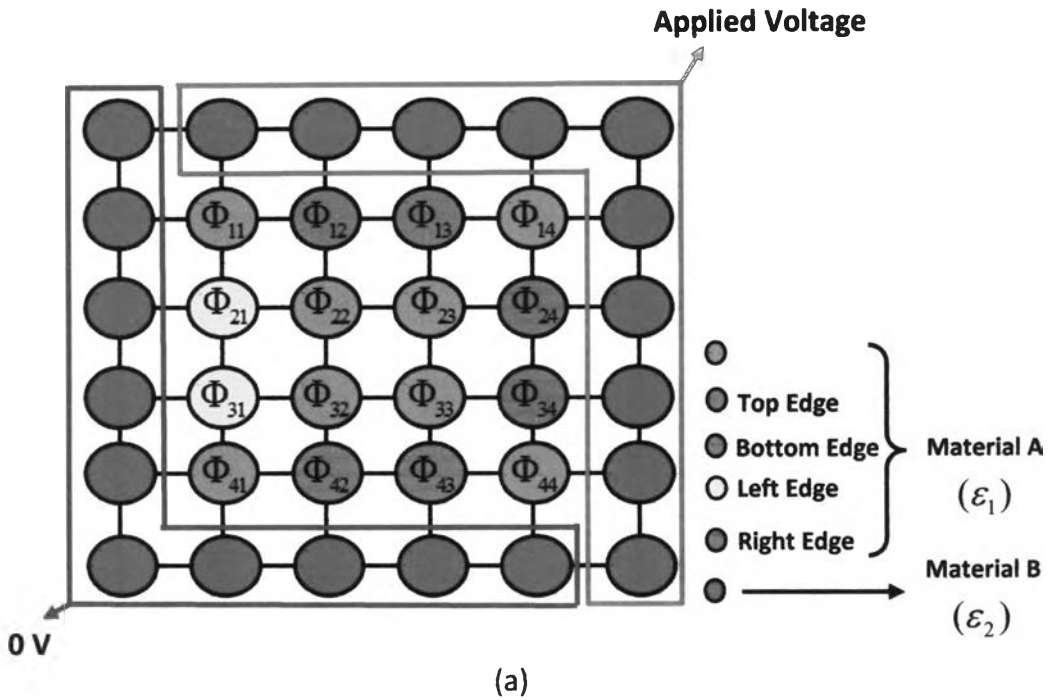


**Figure 3.23** Comparison of the formula between potential element and electric field element. The potential  $\Phi(x, y)$  was obtained from four surrounding nodes, but the electric field was obtained from two adjacent node in the horizontal line for  $E_x$  and vertical line for  $E_y$ .

$$\begin{aligned} \text{at } \Phi_{12}, \quad 4\Phi_{12} &= \Phi_{11} + \Phi_{13} + \Phi_{22} + V_y(\text{boundary}) \\ \text{at } \Phi_{22}, \quad 4\Phi_{22} &= \Phi_{12} + \Phi_{21} + \Phi_{23} + \Phi_{32} \\ \text{at } \Phi_{32}, \quad 4\Phi_{32} &= \Phi_{31} + \Phi_{33} + \Phi_{22} + 0V(\text{boundary}) \end{aligned} \quad (3.26)$$

In the case of electric field system in this thesis work (Figure 3.19), one material with dielectric constant  $\epsilon_1$  was embedded in larger material with dielectric constant  $\epsilon_2$ , two materials have rectangular shapes. All boundary conditions of embedded materials must be calculated (top, bottom, left, and right edge).



(a)

-4	1	0	0	1	0	0	0	0	0	0	0	0	0	0	0	0	0	0	0	$\Phi_{11}$
$-\epsilon_2(\epsilon_1 + \epsilon_2)$	$-\epsilon_1$	0	0	1	0	0	0	0	0	0	0	0	0	0	0	0	0	0	0	$\Phi_{12}$
0	$-\epsilon_2(\epsilon_1 + \epsilon_2)$	$-\epsilon_1$	0	0	1	0	0	0	0	0	0	0	0	0	0	0	0	0	0	$\Phi_{13}$
0	0	1	-4	0	0	0	1	0	0	0	0	0	0	0	0	0	0	0	0	$\Phi_{14}$
1	0	0	$-\epsilon_2(\epsilon_1 + \epsilon_2)$	$-\epsilon_1$	0	0	1	0	0	0	0	0	0	0	0	0	0	0	0	$\Phi_{21}$
0	1	0	0	1	-4	1	0	0	1	0	0	0	0	0	0	0	0	0	0	$\Phi_{22}$
0	0	1	0	0	1	-4	1	0	0	1	0	0	0	0	0	0	0	0	0	$\Phi_{23}$
0	0	0	1	0	0	$-\epsilon_1(\epsilon_1 + \epsilon_2)$	$-\epsilon_2$	0	0	1	0	0	0	0	0	0	0	0	0	$\Phi_{24}$
0	0	0	0	1	0	0	$-\epsilon_2(\epsilon_1 + \epsilon_2)$	$-\epsilon_1$	0	0	1	0	0	0	0	0	0	0	0	$\Phi_{31}$
0	0	0	0	0	1	0	0	1	-4	1	0	0	1	0	0	0	0	0	0	$\Phi_{32}$
0	0	0	0	0	0	1	0	0	1	-4	1	0	0	1	0	0	0	0	0	$\Phi_{33}$
0	0	0	0	0	0	0	1	0	0	$-\epsilon_1(\epsilon_1 + \epsilon_2)$	$-\epsilon_2$	0	0	1	0	0	0	0	$\Phi_{34}$	
0	0	0	0	0	0	0	0	1	0	0	0	-4	1	0	0	0	0	0	0	$\Phi_{41}$
0	0	0	0	0	0	0	0	0	0	1	0	0	$-\epsilon_1(\epsilon_1 + \epsilon_2)$	$-\epsilon_2$	0	0	0	0	$\Phi_{42}$	
0	0	0	0	0	0	0	0	0	0	0	1	0	$-\epsilon_1(\epsilon_1 + \epsilon_2)$	$-\epsilon_2$	0	0	0	0	$\Phi_{43}$	
0	0	0	0	0	0	0	0	0	0	0	0	1	0	0	1	-4	0	0	0	$\Phi_{44}$

=

$b_{11}$
$b_{12}$
$b_{13}$
$b_{14}$
$b_{21}$
$b_{22}$
$b_{23}$
$b_{24}$
$b_{31}$
$b_{32}$
$b_{33}$
$b_{34}$
$b_{41}$
$b_{42}$
$b_{43}$
$b_{44}$

Top Edge
  Bottom Edge
  Left Edge
  Right Edge

(b)

**Figure 3.24** Schematic diagram of (a) 6×6 two-dimensional potential system of material a with dielectric constant  $\epsilon_1$  embedded in the larger material with dielectric constant  $\epsilon_2$ . The voltages are applied at top and right edge of potential system. (b) The linearly matrix equation corresponding to the system, in form of  $AX = B$ .

Some matrix element in the specification matrix A corresponding to these regions will be adjusted, which is classified in two groups as follows:

### 1. Top edge and left edge case

- replacing the value -4 in the element  $a_{ij}$ ,  $i = j$  with the summation of dielectric constant of two materials ( $\varepsilon_1 + \varepsilon_2$ )
- replacing the value 1 in the element  $a_{ij}$ ,  $i = j-1$  with the dielectric constant  $-\varepsilon_2$
- replacing the value 1 in the element  $a_{ij}$ ,  $i = j+1$  with the dielectric constant  $-\varepsilon_1$

### 2. Bottom edge and right edge case

- replacing the value -4 in the element  $a_{ij}$ ,  $i = j$  with the summation of dielectric constant of two materials ( $\varepsilon_1 + \varepsilon_2$ )
- replacing the value 1 in the element  $a_{ij}$ ,  $i = j-1$  with the dielectric constant  $-\varepsilon_1$
- replacing the value 1 in the element  $a_{ij}$ ,  $i = j+1$  with the dielectric constant  $-\varepsilon_2$

Note that the above condition is satisfied when the potential at the top and right edge are higher than the potential at the bottom and left edge, respectively.

**Figure 3.24** depicts the example of  $6 \times 6$  two-dimensional potential system. The dimension of free nodes is  $4 \times 4$  which represents as a material A with dielectric constant  $\varepsilon_1$ . The boundary conditions of material A is separated to four groups by different colors (top edge – pink nodes, bottom edge – green nodes, left edge – yellow nodes, and right edge – blue nodes). For nodes at the corner ( $\Phi_{11}$ ,  $\Phi_{14}$ ,  $\Phi_{41}$ , and  $\Phi_{44}$ ), the boundary condition is neglected and considered as a general free nodes (brown nodes), and red nodes are material B with dielectric constant  $\varepsilon_2$ . The voltages are applied at top and right edge of potential system, bottom and left

edge are reference potential (0 V). According to the specification matrix A, some matrix element values are changed. For top edge ( $\Phi_{12}$  and  $\Phi_{13}$ ) and left edge nodes ( $\Phi_{21}$  and  $\Phi_{31}$ ), the matrix element values of  $a_{ij}$  at  $i = j$ ,  $i = j-1$ , and  $i = j+1$  are changed from 1, -4, 1 to  $(\varepsilon_1 + \varepsilon_2)$ ,  $-\varepsilon_2$ , and  $-\varepsilon_1$ , respectively (grey frames). For bottom edge ( $\Phi_{42}$  and  $\Phi_{43}$ ) and right edge nodes ( $\Phi_{24}$  and  $\Phi_{34}$ ), the matrix element values of  $a_{ij}$  at  $i = j$ ,  $i = j-1$ , and  $i = j+1$  are changed from 1, -4, 1 to  $(\varepsilon_1 + \varepsilon_2)$ ,  $-\varepsilon_1$ , and  $-\varepsilon_2$ , respectively (red frames).

Following to these processes, both the specification matrix A and the boundary matrix B are successfully investigated. The linearly matrix equation  $AX = B$  of two-dimensional electric field system can be solve by inverse matrix method,  $X = A^{-1}B$ . Thus, the potential  $\Phi(x, y)$  was then obtained all over regions of the system. Finally, the desired electrical parameters were determined from Eq. (3.23) to give an electric field distribution throughout the surface area of QDs structure.

### 3.2.3 Results and Discussion

The Matlab® programming language was used again to numerically solve the potential  $\Phi(x, y)$  by FDM method with boundary conditions, which leads to the information of electric field distribution over the two-dimensional electric field system. For testing the results, two-dimensional electric field system like **Figure 3.18** was estimated by two rectangular QDs with the same size ( $8 \times 8$  mesh elements) and spacing between them (18 mesh elements) embedded in GaAs capping layer following to **Figure 3.19**. The dimension of mesh for calculation is  $9801 \times 9801$  which gets close the limitation of program before an error is occurred about the “out of memory” situation. Remind that an accuracy of the calculation depends on the number of mesh, the high number of mesh is used, the precisely results are given. The dielectric constant of two materials were chosen which were different from

## 3-D Potential Distribution

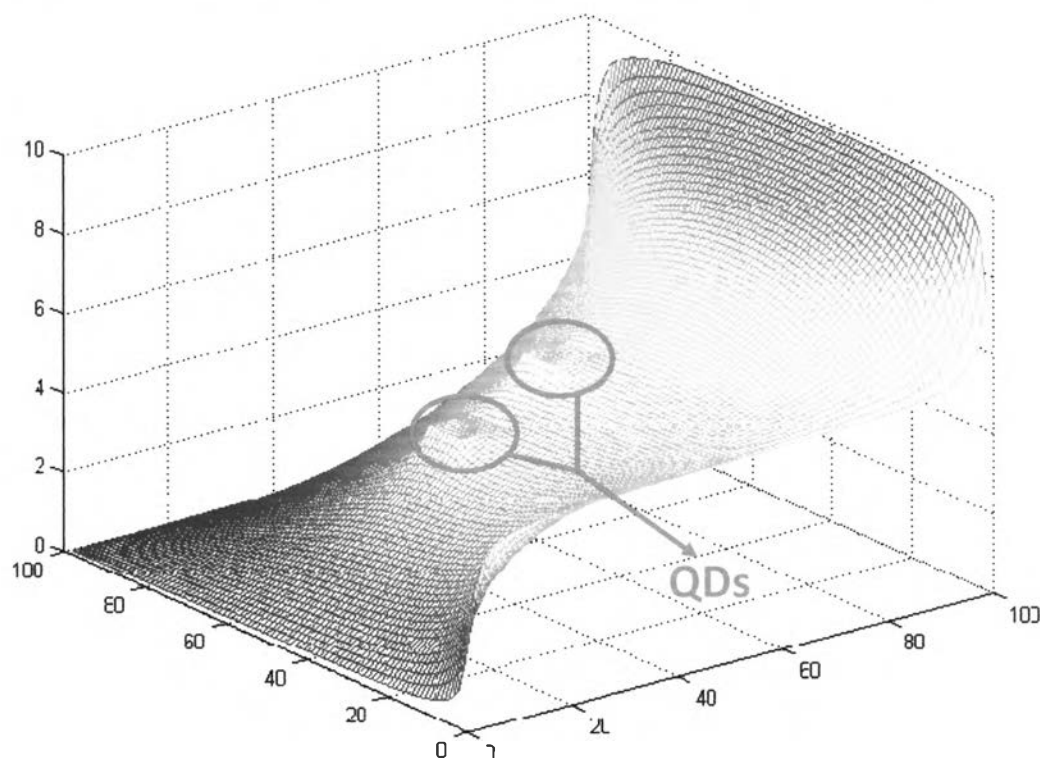


**Figure 3.25** Three-dimensional contour of potential distribution of two QDs embedded in GaAs capping layer corresponding to the two-dimensional system by Matlab® programming.

their original values to clearly observe, especially at the edge of InAs QDs region. Therefore, the dielectric constant value of one material should be much larger than another material, so the dielectric constant of InAs QDs and GaAs capping layer was assumed to  $\epsilon_r = 5000$  and 10, respectively. The magnitude of electric field was adjustable via voltage controlling in the x and y direction, which were applied at top and right edge of potential system, bottom and left edge are reference potential (0 V). This allows controlling an electric field for the desired direction.

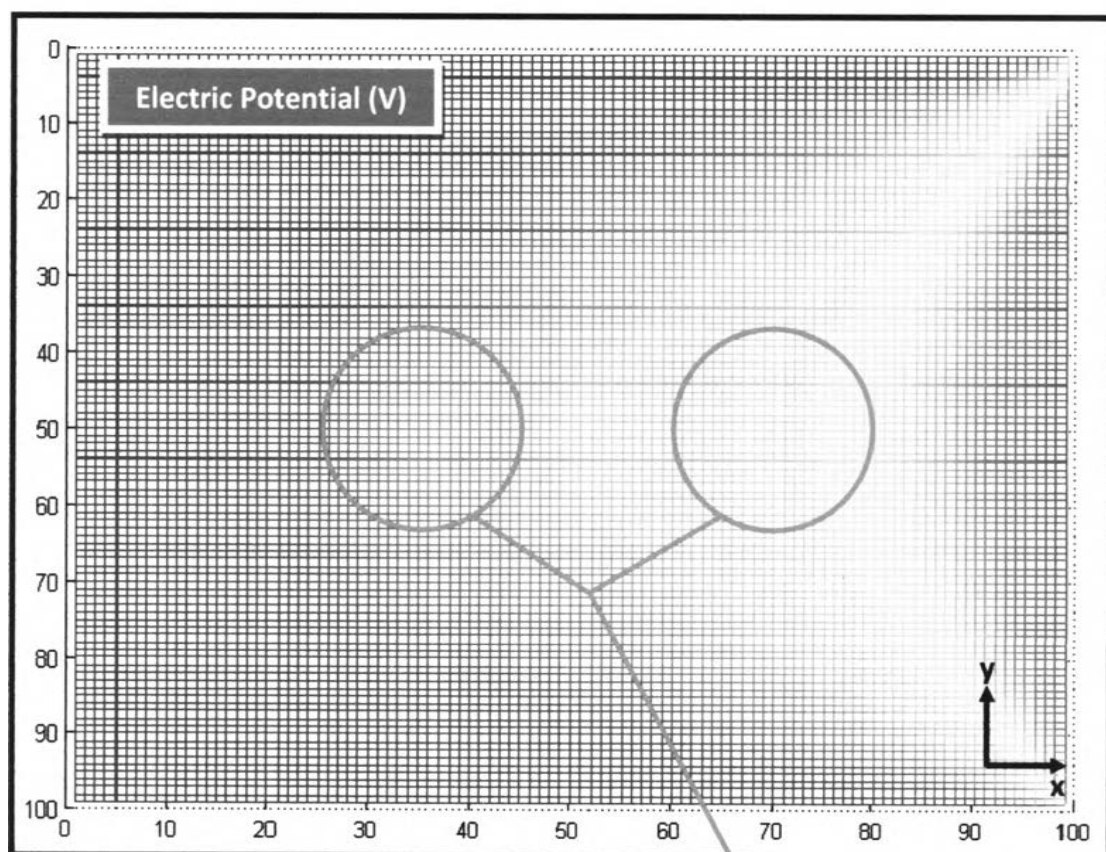
To get the results, Eq. (3.20) and Eq. (3.23) have solved in Cartesian coordinate. This was done by using the double symmetry of the geometric shape and then taking into account of both external (GaAs's edge) and internal (InAs's edge) boundary conditions. In Matlab® it is possible to plot this solution in form of the contour regions, so the potential distribution was shown instead of electric distribution since it is easier to observe and compare the results with the COMSOL programming. The result was shown in **Figure 3.25** as the 3-D potential distribution of the system. The convex regions represent two QDs and other regions are GaAs capping layer area. The reason for distinguished QDs regions is because dielectric constant of QDs is higher than the GaAs capping layer, electric field was permitted passing in QDs greater than GaAs region. Thus, the different of electric field values were explicitly appeared at the interface between two materials.

For checking the exactness of this method, three different cases of applied voltage were demonstrated covering at all possible situations as follows;

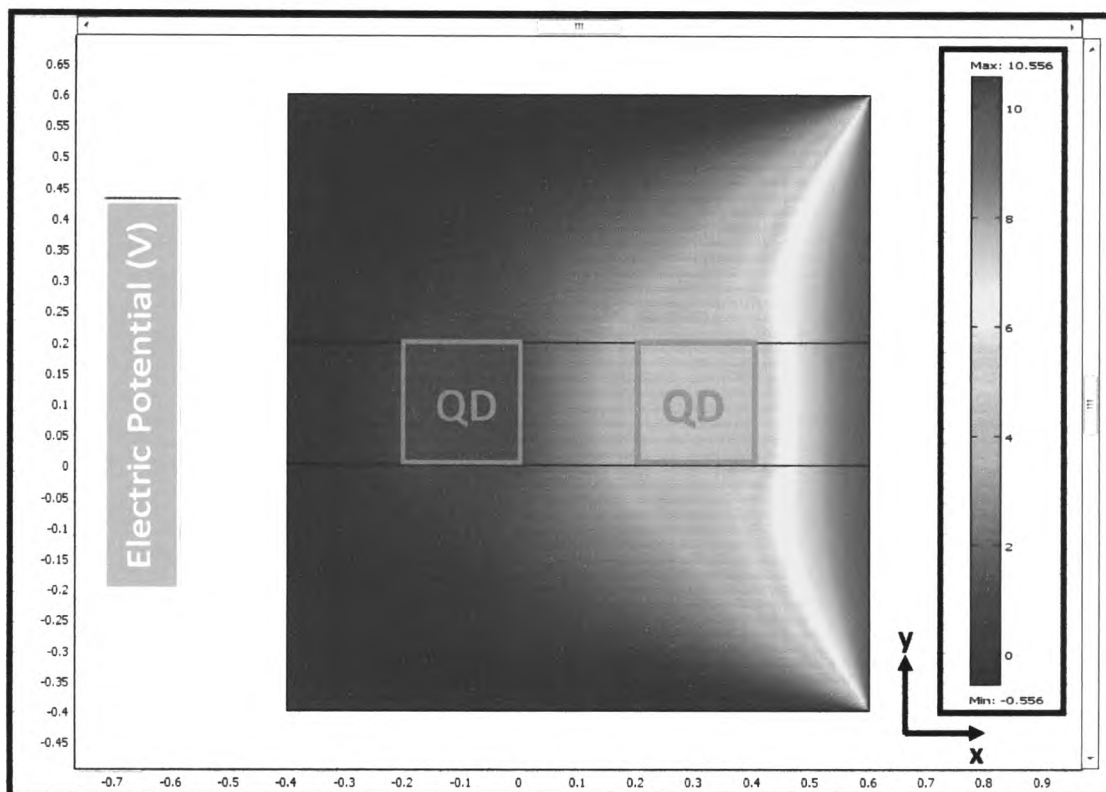
- Case 1: voltage was applied only in the x direction with the magnitude of 10 V.
- Case 2: voltage was applied only in the y direction with the magnitude of 10 V.
- Case 3: voltage was applied both x and y direction with the magnitude of 10 and 5 V, respectively.

The results were shown in **Figure 3.26 - 3.28**, and analysis will be discussed concurrently with the COMSOL's results for comparison in the next article.

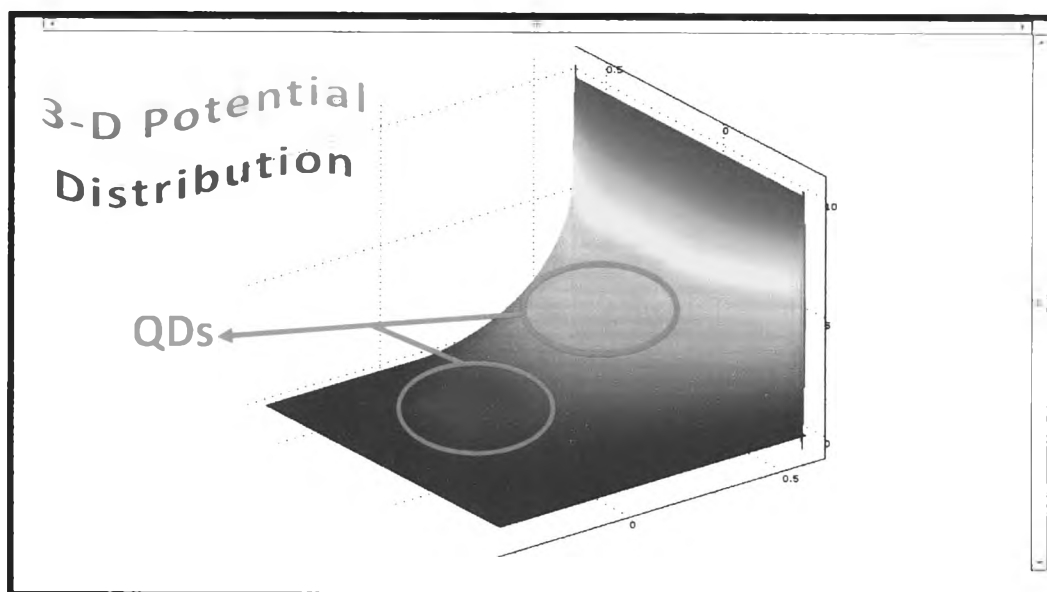




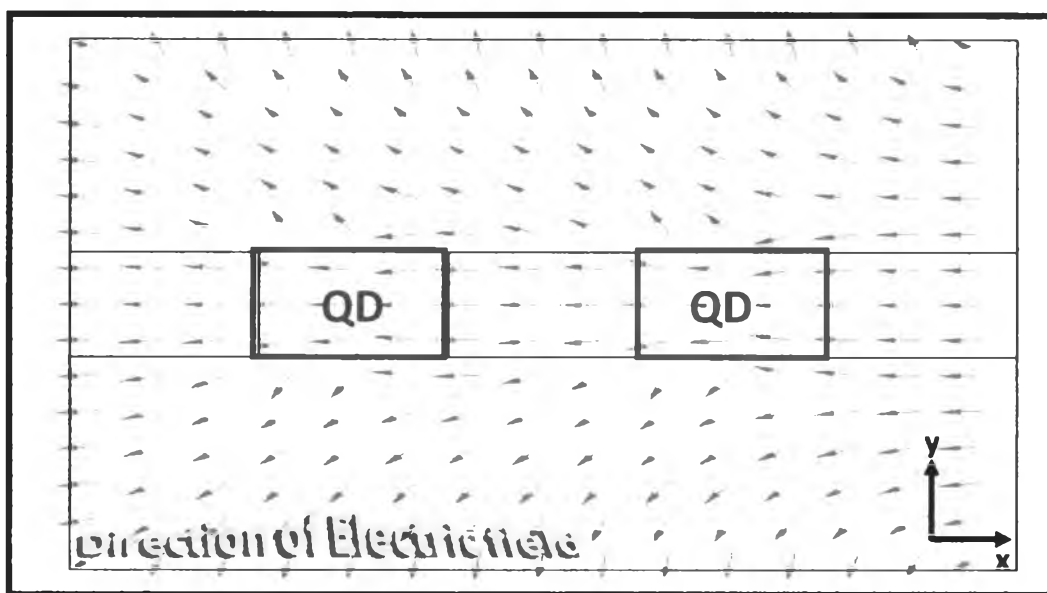
(a) QDs



(b)

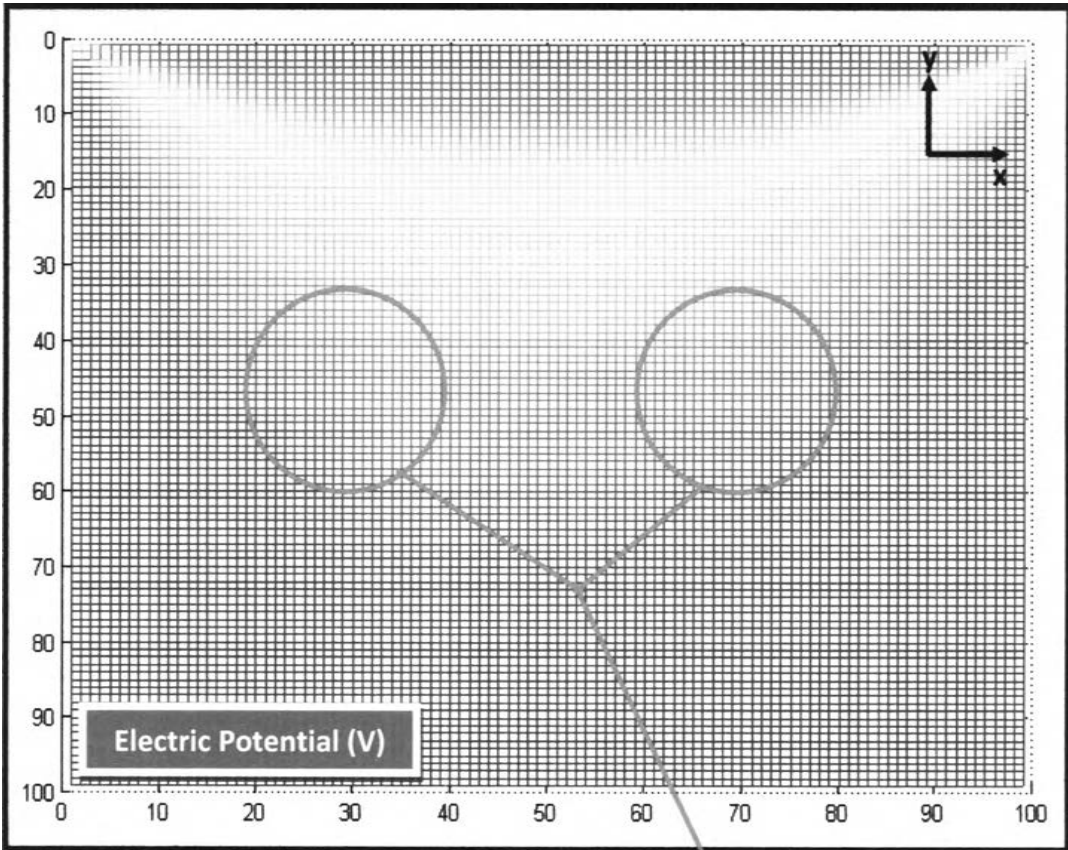


(c)

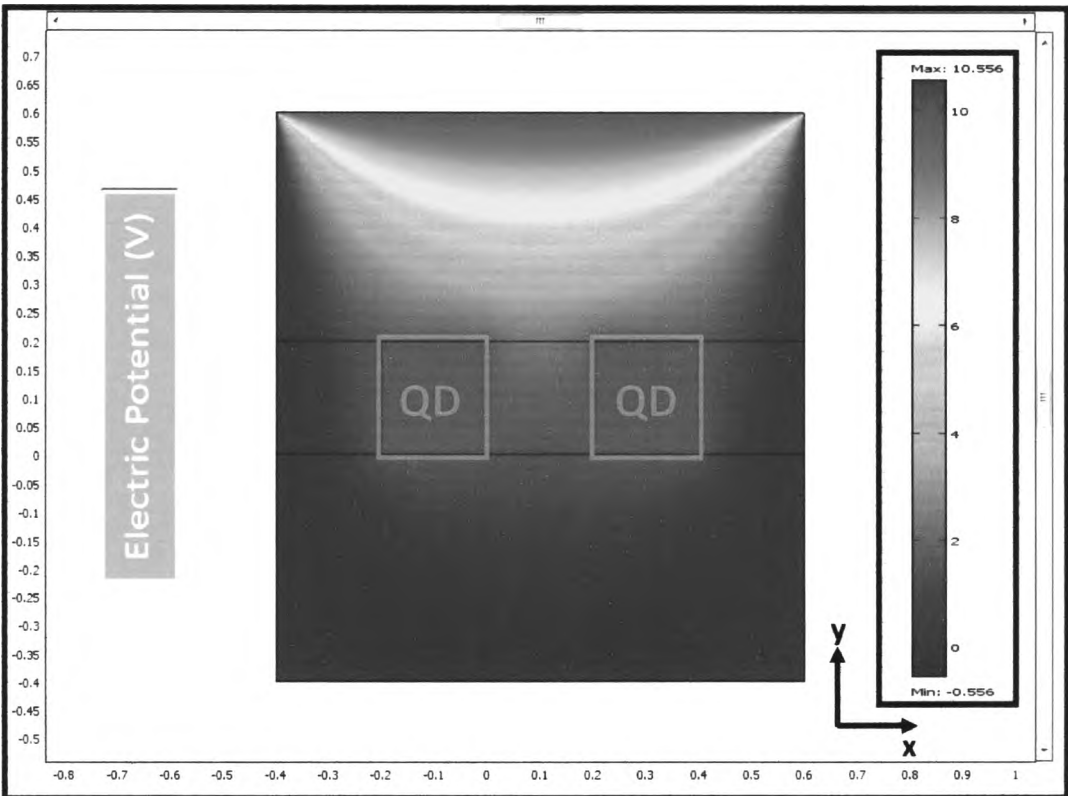


(d)

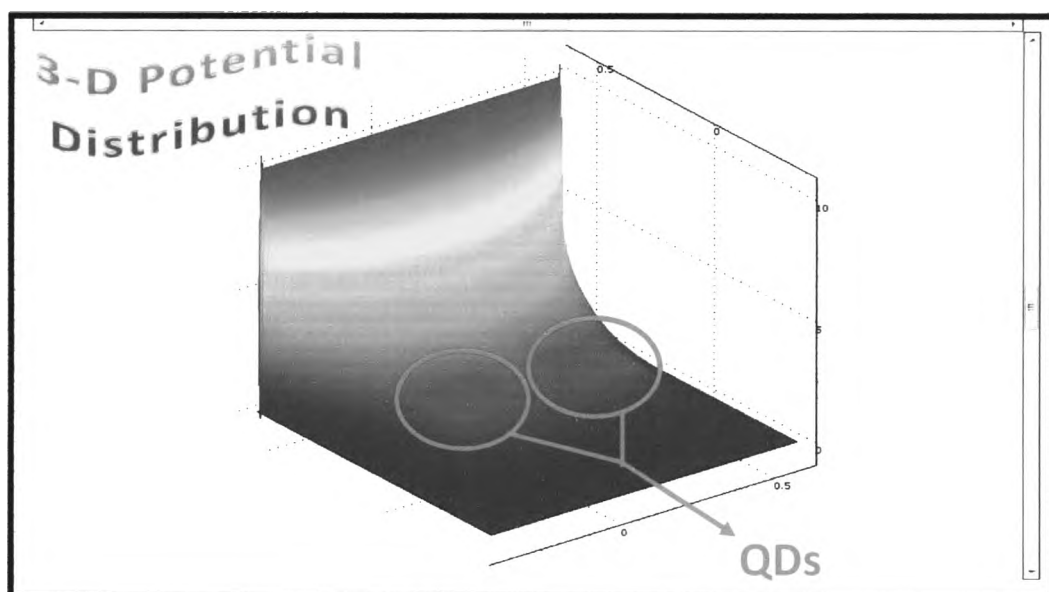
**Figure 3.26** Comparison of two-dimensional potential distribution between (a) Matlab® and (b) COMSOL programming in case of voltage was applied only in the x direction with the magnitude of 10 V. (c) Three-dimensional contour of potential distribution and (d) distribution of electric field's direction represented as the red arrows with normalized magnitude.



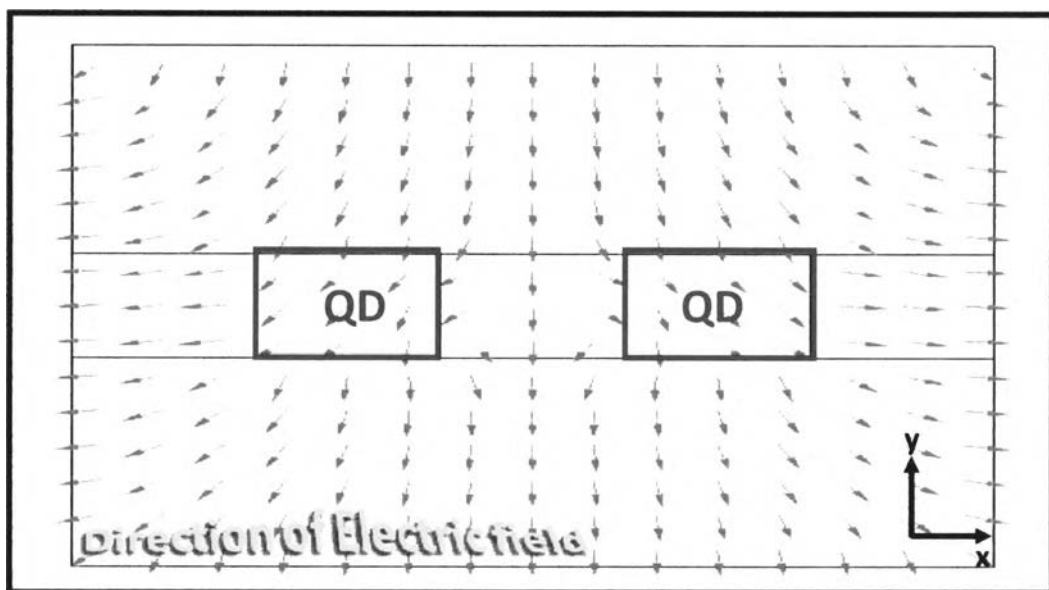
(a) QDs



(b)

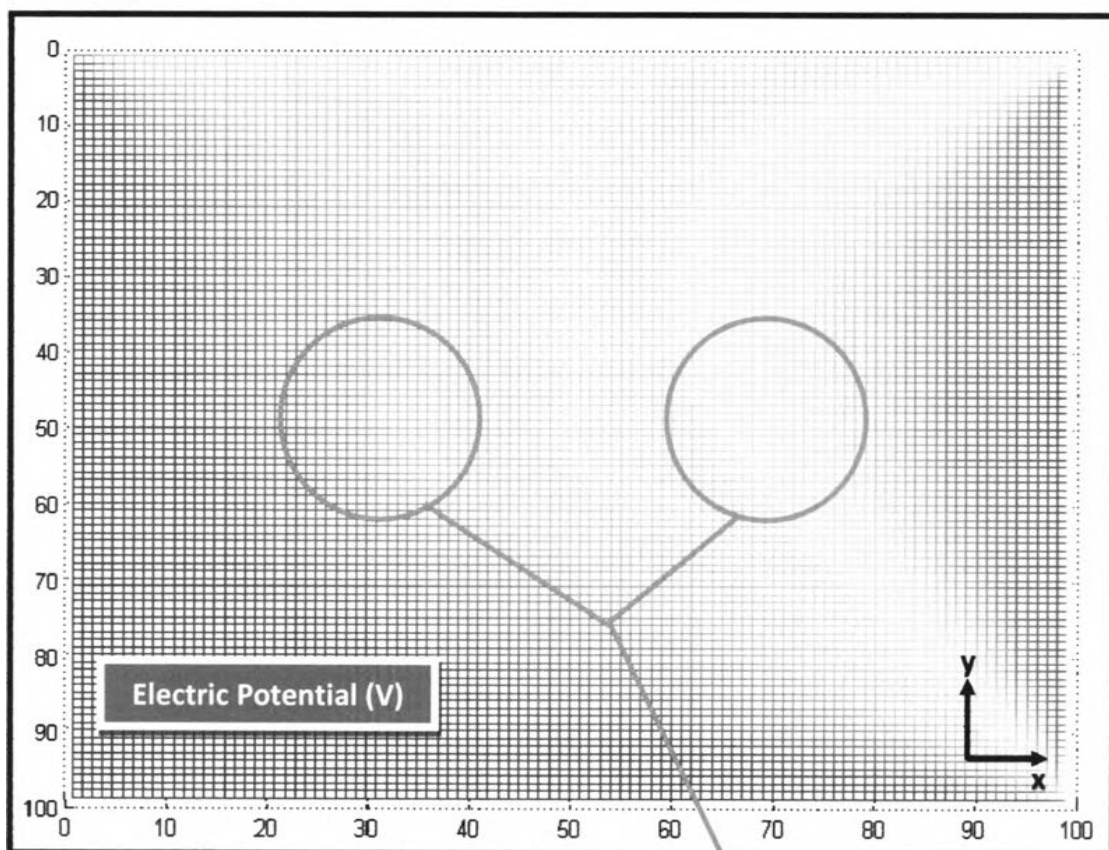


(c)

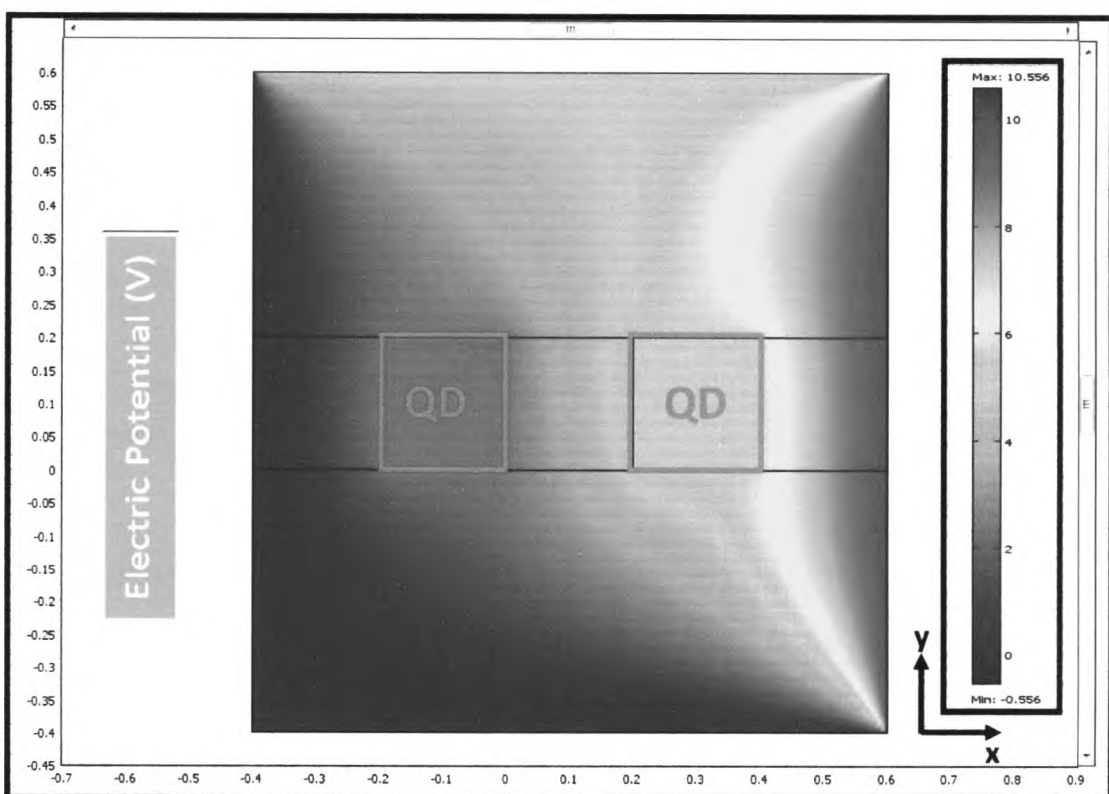


(d)

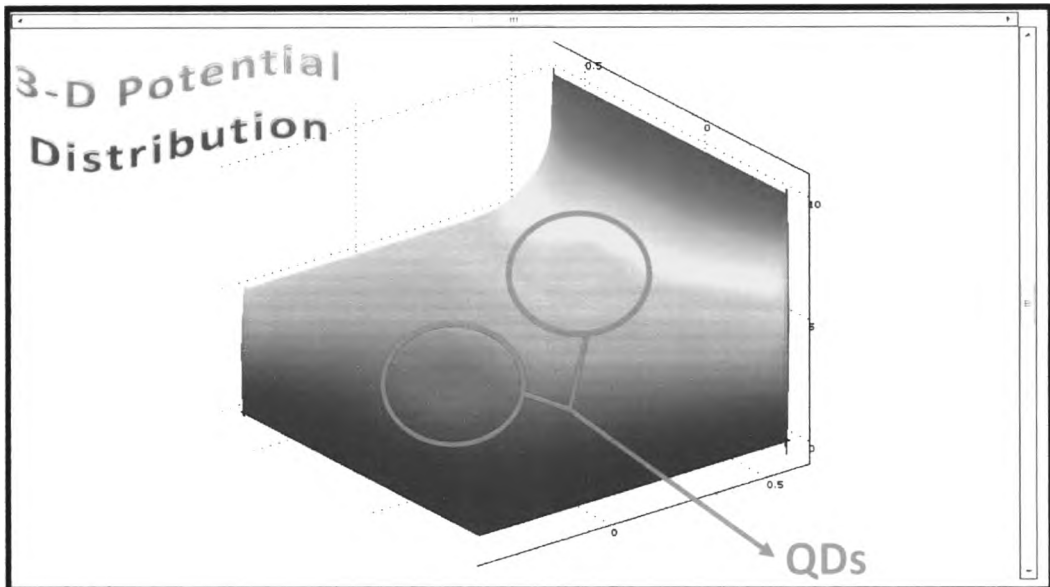
**Figure 3.27** Comparison of two-dimensional potential distribution between (a) Matlab® and (b) COMSOL programming in case of voltage was applied only in the y direction with the magnitude of 10 V. (c) Three-dimensional contour of potential distribution and (d) distribution of electric field's direction represented as the red arrows with normalized magnitude.



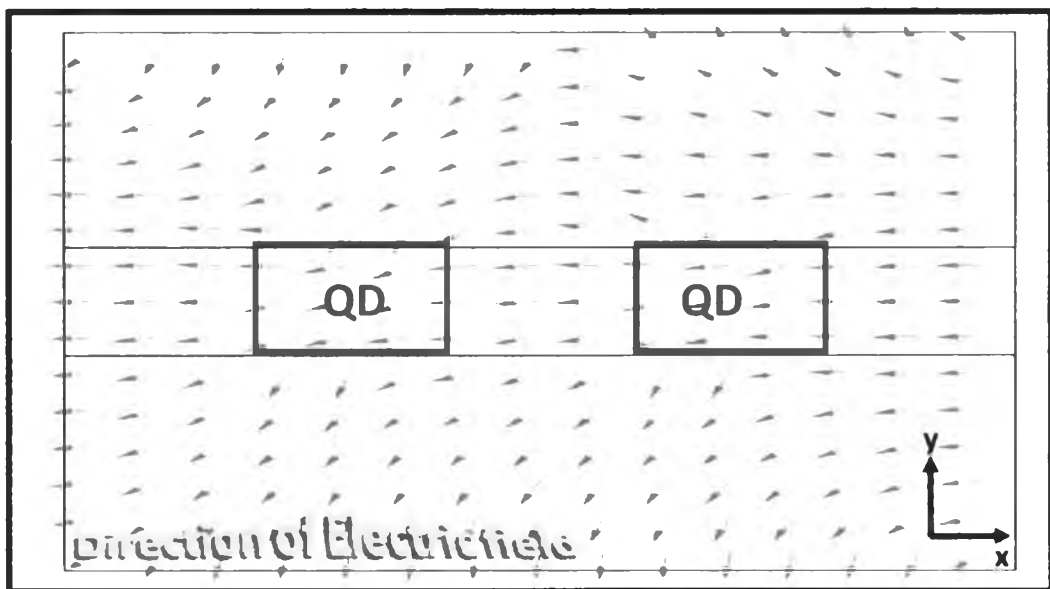
(a) QDs



(b)



(c)



(d)

**Figure 3.28** Comparison of two-dimensional potential distribution between (a) Matlab® and (b) COMSOL programming in case of voltage was applied both x and y direction with the magnitude of 10 and 5 V, respectively. (c) Three-dimensional contour of potential distribution and (d) distribution of electric field's direction represented as the red arrows with normalized magnitude.

### Comparison with COMSOL results

To examine an accuracy of the results, COMSOL programming was utilized again for comparison with the Matlab®'s results. In COMSOL programming, we used electrostatics model in AC/DC module to investigate the potential distribution. The two-dimensional structure was drawn with the same as simulation in Matlab® programming. For subdomains settings, the dielectric constants of two materials were used with the same parameters as discussion before. Similar to boundary settings, the conditions were the same as mentioned in Eq. (3.22) for continuity of electric flux density  $D$  and the same applied voltage in three different cases. The method investigated for solving the problem was using Lagrange quadratic solver [229], with 60 mesh elements in the FDM solution.

The simulation results were revealed in **Figure 3.26 – 3.28**, showing the comparison of two-dimensional potential distribution between Matlab® and COMSOL programming in different three cases of applied voltage. In the first case, voltage was applied along the x direction with magnitude of  $V_x=10$  V, and the electric potential distribution calculated from Matlab® programming was depicted in **Figure 3.26 (a)**. Note that this figure displays two-dimensional plane (x-y) of three-dimensional potential distribution contour in order to be easy for comparison. The electric potential intensity was spreading from the parabolic region closed to voltage source which potential intensity was high in this region (red color) to other parabolic regions which potential intensity was decreased when distance between any potential point  $\Phi(x,y)$ , and voltage source was increased (yellow and green color, respectively). The remnant region was mostly occupied a low intensity of  $\Phi(x,y)$  represent by a blue color. This result was similar to the COMSOL's result as shown in **Figure 3.26 (b)**, the brown square represented QDs region. Concentration to QD in the green region, electrical potential at the end of this region closed to the edge of QD was extended into the end of neighboring regions (yellow and blue region). Because the difference of dielectric constant between two materials which is

remarkable at the interface between them, so changing of  $\Phi(x,y)$  at QDs's edge obviously affected to their neighborhood, same as QD in the blue region (but this case is hardly observed due to low contradiction of color). **Figure 3.26 (c)** displays three-dimensional potential distribution contour from COMSOL programming, the brown circles was two convex regions represented two QDs, same as the results simulated by Matlab® (**Figure 3.25**). **Figure 3.26 (d)** shows distribution of electric field's direction in two-dimensional plane ( $x$ - $y$ ), red arrows represent the normalized magnitude of electric field, and the blue frames are two QDs region. Electric field was broadening from voltage source to the three boundaries which are reference voltage, following to the transfusion of electrical potential. The electric field at the edge of QDs region was a little different from other region since the effect of dielectric constant, which is same reason as described previously in **Figure 3.26 (a)**.

In the second case, voltage was applied along the  $y$  direction with magnitude of  $V_y=10$  V. The result of two-dimensional potential distribution were depicted in **Figure 3.27 (a) and (b)**, which were similar to the first case shown in **Figure 3.26 (a) and (b)** by rotating their pictures to  $90^\circ$  counterclockwise. The three-dimensional potential distribution contour in **Figure 3.27 (c)** was also the same as **Figure 3.26 (c)**, but changing the voltage distribution into  $y$  axis. The distribution of electric field's direction in two-dimensional plane (**Figure 3.27 (d)**) was nearly in **Figure 3.26 (d)**. Nevertheless, a little difference was appeared at the QDs region by electric field's direction in both QDs was opposite as a reflected image of each other from a mirror (or image charges arrangement [228]), but in **Figure 3.27 (d)** the electric field's direction in two QDs was the same alignment. This implied that the different direction of applied voltage caused the different of electric field's distribution in aligned QDs, which probably influenced to the inside carriers, following to QCSE. Moreover, the effect was more explicit by increasing the number of QDs to become a long chain QDs in order to compare between the effect of electric field along the QDs alignment and other directions. The reasons for all results in this case can be described in the same way with the first case.



In the last case, voltage was applied both x and y direction with the magnitude of 10 and 5 V, respectively, and the results were shown in **Figure 3.28**. The potential distribution contour shown in **Figure 3.28 (a)** was different from two previous cases. There was a cross section of one dimensional vortex prominently appeared in three regions (green, yellow, and blue colors), same as the COMSOL's results shown in **Figure 3.28 (b)**. **Figure 3.28 (d)** shows distribution of two-dimensional electric field's direction, the result was more complicated than two previous cases since there are two voltage sources applied in different direction. The electric field distribution in this case was mostly influenced from the voltage source in the x direction because its voltage was higher than the voltage source in the y direction. The electric field distribution at nearly voltage source in the x direction were three different forms; the electric field was broadening to the reference voltage at  $-x$  and  $-y$  direction, and moving up to the voltage source in the y direction because of higher potential energy. The electric field distribution from voltage source in the y direction mostly was broadening to the reference voltage at  $-x$  direction. In QD region, the electric field distribution was similar to the first case though some of it was scribbled, but overall distribution was moved toward the  $-x$  direction.

### 3.3 CONCLUSION

In the first part of this chapter, we have demonstrated the degree of linear polarization (PD) emitted from the two-dimensional aligned QD system which were theoretically calculated by using the Schrödinger equation implemented with the finite-difference method (FDM). The results were summarized as follows:

- In case of single QD, an isotropic QD shape exhibits a zero degree of polarization. A certain degree of polarization anisotropy is obtained when the dot is elongated in one direction and can be enhanced by increasing its aspect ratio.

- For aligned QDs system, the higher number of QDs gives an enhanced polarization degree due to the stronger coupling effect of their wavefunctions (exchange interactions during the recombination process determines whether or not the polarization of the light gives rise to a larger value). The polarization strength strongly depends on spatial separation between adjacent dots. When the interdot spacing is smallest (completely QDs attachment), the highest degree of polarization is manifested. In addition, the size of the individual quantum dots also affects the degree of polarization, i.e., reducing the QD size give a large degree of coupling, thus, a large degree of polarization. Absolutely, a large number of QDs linearly aligned with a small dot size and a very close spacing between adjacent dots are able to eliminate of all other polarization components and produce more an emission light in a one certainly direction.

In the second part, the two-dimensional electric field system was modeled in order to apply for the aligned QDs system. Improvement of electric field by solving numerically the 2-D Laplace's equation with FDM method provides more realistically

potential distribution, as a result, the precisely electric field distribution is obtained. This enables to adjust the electric field distribution in preferred direction via such an axially applied voltage.

The results of calculation from two parts mentioned above were confirmed the validity by means of comparison the calculated results between Matlab® programming language and COMSOL Multiphysics. Combining the aligned QDs system with the applied electric field system allows us to study QCSE on polarization degree. This is critical for describing how electric field affects the behavior of carrier interaction and subsequently the change in coupling strength has on polarization degree. A clear understanding of the polarization characteristics of coupled quantum dots is a crucial step toward controlling of the emission light in the operation of optoelectronic devices. In chapter 4 the all calculation results of applied electric field on aligned QDs system will be discussed in great details.